Clim. Past Discuss., 9, 4655–4704, 2013
www.clim-past-discuss.net/9/4655/2013/
doi:10.5194/cpd-9-4655-2013

Climate of the Past Discussions
Open Access

NGRIP CH_4 concentration from 120 to 10 kyr before present and its relation to a $\delta^{15}N$ temperature reconstruction from the same ice core

M. Baumgartner[1], P. Kindler[1], O. Eicher[1], G. Floch[2,3], A. Schilt[1], J. Schwander[1], R. Spahni[1], E. Capron[4,5], J. Chappellaz[2,3], M. Leuenberger[1], H. Fischer[1], and T. F. Stocker[1]

[1]Climate and Environmental Physics, Physics Institute, and Oeschger Centre for Climate Change Research, University of Bern, Sidlerstrasse 5, 3012 Bern, Switzerland
[2]CNRS, Laboratoire de Glaciologie et Géophysique de l'Environnement (LGGE), 38041 Grenoble, France
[3]Univ. Grenoble Alpes, Laboratoire de Glaciologie et Géophysique de l'Environnement (LGGE), 38041 Grenoble, France
[4]British Antarctic Survey, NERC, High Cross, Madingley Road, Cambridge, CB3 0ET, UK
[5]Insitut Pierre-Simon Laplace/Laboratoire des Sciences du Climat et de l'Environnement, UMR8212, CEA-CNRS-UVSQ, 91191 Gif-sur-Yvette, France

Received: 11 July 2013 – Accepted: 5 August 2013 – Published: 14 August 2013

Correspondence to: M. Baumgartner (baumgartner@climate.unibe.ch)

Published by Copernicus Publications on behalf of the European Geosciences Union.

Abstract

During the last glacial cycle, Greenland temperature showed many rapid temperature variations, the so called Dansgaard-Oeschger (DO) events. The past atmospheric methane concentration closely followed these temperature variations, which implies that the warmings recorded in Greenland were probably hemispheric in extent. Here we substantially extend and complete the North Greenland Ice Core Project (NGRIP) methane record from Termination 1 back to the end of the last interglacial period with a mean time resolution of 54 yr. We relate the amplitudes of the methane increases associated with DO events to the amplitudes of the NGRIP temperature increases derived from stable nitrogen isotope (δ^{15}N) measurements, which have been performed along the same ice core. We find the sensitivity to oscillate between 5 parts per billion by volume (ppbv) per °C and 18 ppbv °C^{-1} with the approximate frequency of the precessional cycle. A remarkably high sensitivity of 25.5 ppbv °C^{-1} is reached during Termination 1. Analysis of the timing of the fast methane and temperature increases reveals significant lags of the methane increases relative to NGRIP temperature for the DO events 5, 9, 10, 11, 13, 15, 19, and 20. We further show that the relative interpolar concentration difference of methane is 4.6 ± 0.7 % between the DO events 18 and 19 and 4.4 ± 0.8 % between the DO events 19 to 20, which is in the same order as in the stadials before and after DO event 2 around the Last Glacial Maximum.

1 Introduction

Methane (CH_4) is a potent greenhouse gas with preindustrial atmospheric concentrations changing between 350 and 750 ppbv over the last 800 thousand years (kyr) before present (BP) (Loulergue et al., 2008). This statement is based on the measurements along polar ice cores, a unique archive to reconstruct the range of the past atmosphere. Human activity has increased the atmospheric abundance of CH_4 from the preindustrial Holocene level of 750 ppbv to around 1800 ppbv through the last 200 yr

CPD
9, 4655–4704, 2013

(Etheridge et al., 1998). The maximum increase rate under the anthropogenic influence of 17 ppbv yr^{-1} was observed in 1981 (Etheridge et al., 1998). Ice core measurements over the last glacial cycle revealed numerous fast and strong variations in the CH_4 concentration, when only natural sources have been present. However, the maximum increase rate observed during the last glaciation and deglaciation of up to 2.5 ppbv yr^{-1} (Chappellaz et al., 2013) is far below the maximum increase rate under the anthropogenic influence. Although atmospheric CH_4 concentrations can be readily measured using polar ice cores, important questions concerning the location and strength of the different sources and sinks and the sensitivity of the emissions to climate change are still open.

The major natural sources of CH_4 are wetlands (Spahni et al., 2011), where archaea produce CH_4 by the degradation of organic material under anaerobic conditions (e.g. Bridgham et al., 2013). The absence of molecular oxygen is crucial for methanogenesis, underlining the importance of water in the source regions acting as a gas barrier. Given anoxic conditions in wetland areas the CH_4 production rate generally increases with increasing temperature (Christensen et al., 2003; Walter et al., 2001; Ringeval et al., 2013; Zürcher et al., 2013). The amount of CH_4 released to the atmosphere is thus sensitive to the temperature at the wetland source location. Precipitation determines wetland extent and water saturation of the soil and thus also influences the global CH_4 source strength (Bloom et al., 2010). Bottom-up models of methane emission further suggest that net primary productivity regulates the carbon pool available for methanogenesis, and thus CH_4 production and emissions (Melton et al., 2013; Wania et al., 2012). After its emission, CH_4 is mixed in the global atmosphere within a few years, leading to a relatively uniform concentration distribution. Under present day conditions, it takes on average 8.7 ± 1.3 yr to decrease the CH_4 concentration in the atmosphere by a factor e (Denman et al., 2007), through oxidation in the troposphere by its major sink, the OH radical. We assume a minor influence of variations in the sink strength to the atmospheric CH_4 budget during the last glacial cycle, in line with recent results of atmospheric chemistry modeling studies (Levine et al., 2011, 2012).

CPD
9, 4655–4704, 2013

Both, the strongest source and sink strengths are found in the tropical regions, but also boreal wetlands contribute substantially to the global emissions (Spahni et al., 2011). The Northern Hemisphere dominates the emissions due to its larger land area compared to the Southern Hemisphere, which leads to asymmetry of the latitudinal source distribution and to an interpolar concentration difference also documented based on the past atmospheric composition in bipolar ice core studies (e.g. Baumgartner et al., 2012; Brook et al., 2000; Chappellaz et al., 1997).

During the last glacial cycle, Greenland temperature experienced many rapid and strong variations (NGRIP Project Members, 2004), the so called DO events (Dansgaard et al., 1982). While the northward heat transport by the Atlantic Meridional Overturning Circulation (AMOC) of the ocean plays a key role in producing such variations (Stocker and Johnsen, 2003), also more regional processes, such as the sudden collapse of the sea ice coverage in the Nordic Sea, may contribute to the amplitude and speed of the changes (Li et al., 2010; Petersen et al., 2013). It has been shown that the correlation between Greenland temperature and CH_4 concentration is extraordinarily strong (Huber et al., 2006; Brook et al., 1996) and that therefore the warmings recorded in Greenland likely have a hemispheric extent (Voelker, 2002; Clement and Peterson, 2008).

Qualitative temperature reconstructions are available from stable water isotope ($\delta^{18}O$, δD) measurements along polar ice cores. However, quantitative temperature estimates based on the relationship between $\delta^{18}O$ and temperature are limited for Greenland ice due to the influence of precipitation seasonality and source temperature changes (Krinner et al., 1997; Boyle, 1997). The isotopic composition of nitrogen trapped in the air bubbles in the ice is able to quantitatively constrain the magnitude of the fast temperature increases (Severinghaus et al., 1998; Severinghaus and Brook, 1999; Lang et al., 1999). Nitrogen is an inert gas and its isotopic composition ($\delta^{15}N$) in the atmosphere is thus assumed to be constant over time. Due to gravitational fractionation in the firn column of an ice sheet, $\delta^{15}N$ is increased at the bottom of the firn where air bubbles are enclosed in the ice (lock-in depth) compared to the atmospheric

CPD
9, 4655–4704, 2013

concentration. A rapid temperature increase at the surface of an ice sheet leads to the establishment of a temperature gradient in the firn. Because gases diffuse in the firn about ten times faster than heat, the temperature gradient initiates thermal gas diffusion and leads to a further increase in $\delta^{15}N$ at the lock-in depth compared to the atmospheric value (Severinghaus et al., 1998) providing a quantitative physical thermometer for fast surface temperature changes on the ice sheet in the past. Neglecting the small difference of diffusion coefficients in air between ^{15}N of N_2 and CH_4, $\delta^{15}N$ will have no age difference with respect to CH_4 and is therefore, in contrast to the stable water isotope temperature proxy, ideally suited for studies on timings and phase relationships (Severinghaus et al., 1998).

Here, we substantially extend and complete the CH_4 record of the NGRIP ice core from Termination 1 ($\sim$ 10 kyr BP) back to the end of the last interglacial period ($\sim$ 120 kyr BP). In Sect. 2 the measurement system for CH_4 concentrations is described and the new and earlier published NGRIP CH_4 data are merged to a consistent concentration scale. In Sect. 3 the new high resolution CH_4 record from NGRIP is presented and related to the $\delta^{15}N$ data (Kindler et al., 2013; Huber et al., 2006; Landais et al., 2004, 2005; Capron et al., 2010a, b, 2012) and the NGRIP temperature reconstruction based on these $\delta^{15}N$ data (Kindler et al., 2013). In particular, we compare the magnitude of the CH_4 increases and the NGRIP temperature increases at the onset of DO events and further investigate the timing between CH_4 and $\delta^{15}N$ increases. Our discussion in Sect. 4 focuses on the implication of our new results on the evolution of the wetland CH_4 sources over the last glacial cycle. Conclusions are given in Sect. 5.

2 Methods

At Bern, in order to determine CH_4 concentrations, the air of ice samples of about 40 g is extracted by a melt-refreeze step and analysed by gas chromatography (e.g. Chappellaz et al., 1997; Flückiger et al., 2004). For NGRIP the samples correspond to a depth interval of about 5 cm. The thermal conductivity detector for the main air

CPD
9, 4655–4704, 2013

components (N_2, O_2 and Ar) and the flame ionization detector for CH_4 are calibrated at hourly intervals with two standard gases (1050 and 408 ppbv). Each calibration is checked by a measurement with a third standard gas. The current standard gas is in use since 2010, and a total of 507 standard measurements show a mean concentration with standard deviation of 529.1 ± 3.1 ppbv, which implies long term stability of the calibration scale. Measurements with standard gases from the National Oceanic and Atmospheric Administration (NOAA) show that the Bern scale is approximately 1 % above the NOAA scale. Blank measurements with air free ice and standard gas reveal a process blank of 10.8 ± 4.6 ppbv. This offset is determined for each extraction vessel separately and is subtracted from each measurement on natural ice. The precision of the measurements on natural ice is determined by reproducibility measurements of natural ice samples at 22 NGRIP depths. In each of the 22 depths, we measured a series of 5 adjacent samples randomly distributed over the different extraction vessels and duration of the measurement series. The standard deviation of the residuals of the 107 reproducibility samples is 5.9 ppbv. Note that 3 measurements have been excluded due to badly sealed vessels. The measured concentrations are not corrected for the ∼ 4 ppbv depletion due to gravitational fractionation in the firn column of an ice sheet, in line with previously published work (e.g. Baumgartner et al., 2012; Schilt et al., 2010a, b; Spahni et al., 2005; Huber et al., 2006). 163 new measurements of the NGRIP core were performed at Laboratoire de Glaciologie et Géophysique de l'Environnement (LGGE) in Grenoble, in parallel to 103 measurements on the Vostok core covering the same time period (Bender et al., 2006). The same technique as in Bern was used but with a standard gas including 499 ppbv of CH_4 (Chappellaz et al., 1997). The standard deviation of the residuals calculated on NGRIP (Vostok) duplicates or triplicates is 2.6 ppbv (4.3 ppbv), respectively.

To check for offsets against previously published NGRIP sections (Capron et al., 2010b, 2012; Schilt et al., 2010b; Huber et al., 2006; Flückiger et al., 2004) an extensive set of remeasurements has been performed together with the new measurements. We subtract the previously measured concentrations, which are obtained by interpolation

CPD
9, 4655–4704, 2013

to the depth of the remeasurements, from the concentration of the remeasurements (summary in Table 1). 41 remeasurements are 2.9 ± 1.9 ppbv (mean of the residuals and standard error of the mean) higher compared to measurements performed in 2004. The values published by Huber et al. (2006) are thus consistent with the new data on the 2σ level. 43 remeasurements reveal an offset of 14.5 ± 1.4 ppbv compared to measurements performed in 2002 (Flückiger et al., 2004) and 31 remeasurements show an offset of 8.4 ± 2.9 ppbv compared to another series of measurements in 2002 (Schilt et al., 2010b). Further, intercomparison of 188 measurements with the CH_4 lab from LGGE Grenoble (Capron et al., 2010b, 2012) yield a current offset of 12.2 ± 1.2 ppbv, which suggests an increase in the Bern–Grenoble correction compared to the last determined value of 6 ppbv (Spahni et al., 2005). The 163 measurements from 2001–2002 by LGGE published in this study are 26.5 ± 1.0 ppbv lower compared to the new measurements from Bern over the same section. Based on this remeasurement statistics, we assume a consistent level of Bern concentrations since the year 2004. NGRIP concentrations measured before 2004 (Flückiger et al., 2004; Schilt et al., 2010b) and concentrations from LGGE Grenoble (Capron et al., 2010b, 2012 and new data) are increased by the specified values to bring all NGRIP concentrations on a common scale.

3 Results

Figure 1 presents 1094 new CH_4 measurements along the NGRIP ice core. The new measurements cover the time intervals of the DO events 5–8, the DO events 13–14, and the DO events 18–25. Together with the previously published 1008 values (Baumgartner et al., 2012; Capron et al., 2010b, 2012; Schilt et al., 2010b; Huber et al., 2006; Flückiger et al., 2004) this completes the NGRIP record from Termination 1 back to the end of the last interglacial period (Marine Isotope Stage – MIS – 5.5, also called the Eemian). The mean time resolution of the record is 54 yr, which is in the same order as

CPD
9, 4655–4704, 2013

the width of the gas age distribution of enclosed air in the NGRIP ice core as calculated after Schwander et al. (1993) and Spahni et al. (2003).

The new dataset provides the most detailed profile obtained by discrete measurements of the evolution of the CH_4 concentration during the last glacial cycle, and can be compared with continuous CH_4 measurements performed on the North Greenland Eemian Ice Drilling (NEEM) ice core (Chappellaz et al., 2013). It shows that the northern concentrations of CH_4 varied in the range between 360 and 780 ppbv during the last glacial cycle (Fig. 2). Apart from the early Holocene and the end of the Eemian, typical interglacial concentrations of more than 640 ppbv are only reached during the DO events 17, 21, 23, and 24, which occur relatively early during the glaciation and also during the Bølling Allerød (BA) period. Similarly, concentrations of lower than 420 ppbv are only reached at the end of the last glacial, in the time period between 30–17 kyr BP around the last glacial maximum (LGM). Before that, the Greenland CH_4 concentration never falls below a relatively stable threshold of 420 ppbv. In fact, 68 % of all the measurements are found in between 460 and 620 ppbv, i.e. within a range of 160 ppbv, with the most frequent concentration to be around 500 ppbv (Fig. 2).

3.1 Methane and NGRIP temperature

The CH_4 concentration shows pronounced variations along with Greenland temperature over the last glacial cycle. Here we use the NGRIP temperature (red curve in Fig. 1) as calculated by Kindler et al. (2013), who applied the firn densification and heat diffusion model from Schwander et al. (1997). In brief, the model input parameters, which are the accumulation rate and the temperature based on $\delta^{18}O$ data, were modified until the measured $\delta^{15}N$ could be reproduced by the model. For more details on the calculation of the temperature record we refer to Kindler et al. (2013).

Figure 1 shows that almost every fast temperature variation has a counterpart in the CH_4 concentration. One exception is found in the temperature peak between the DO events 14 and 15, where no CH_4 variation is found, which is attributed to insufficient data resolution (Huber et al., 2006). Indeed a small CH_4 peak associated with

CPD
9, 4655–4704, 2013

the temperature peak appears in the continuous CH_4 profile on the NEEM ice core (Chappellaz et al., 2013). Similar temperature jumps are associated with different CH_4 amplitudes. A different response to a certain degree of warming is most apparent when comparing DO events 3 and 4. A more quantitative analysis of the amplitudes of the fast temperature and CH_4 increases follows in Sect. 3.2.

Interestingly, during some time periods of slow variations in NGRIP temperature and CH_4 concentration, a decoupling between these two quantities can be observed. During some interstadial periods, e.g. the BA period, temperature shows a decreasing trend over several thousand years, while the CH_4 concentration stays at a rather stable level (Fig. 1). A similar pattern is visible during DO events 7 and 22 and during the first part of DO event 8. Decoupling is also visible during certain stadial periods. In the two thousand years before the onset of the BA period, the slow increase in the CH_4 concentration occurs at a stable NGRIP temperature level. In contrast, the slow early CH_4 increases before the DO events 8 and 12 are positively correlated with the temperature increases. So while a general synchrony between CH_4 and NGRIP temperature exists, a one-to-one coupling cannot be expected as the temperature record is representative for local temperature changes in Greenland, while CH_4 sources respond to climate changes in boreal and tropical regions.

3.2 Amplitudes of CH_4 and temperature

The unambiguous attribution of each fast temperature increase to a fast CH_4 increase allows us to compare the magnitudes of the increases. Here, we define the effective CH_4-to-NGRIP temperature sensitivity μ for the fast increases of the DO events as:

$$\mu = \frac{\Delta CH_4}{\Delta T}, \tag{1}$$

where ΔCH_4 and ΔT are the amplitudes of the fast CH_4 and temperature increases (Fig. 3), respectively. Note that this reflects a covariance of CH_4 concentration to temperature amplitudes at the NGRIP site and should not be mixed up with a local tem-

CPD
9, 4655–4704, 2013

perature sensitivity of CH_4 emissions to the temperature in the wetland source areas. The parameter μ may significantly underestimate the increase in CH_4 emissions as a response to a one degree wetland source temperature warming, since NGRIP temperature amplitudes are influenced by polar amplification (Serreze and Barry, 2011). The underestimation might be particularly strong when the CH_4 sources are not located in high northern latitudes. Note further that other drivers than temperature, such as precipitation and net primary productivity, regulate the total wetland extent and might thus also determine the variations in μ (see Sect. 4.2). Our ice core derived values for μ represent valuable constraints for modelling simulations. Typically, bottom-up wetland CH_4 emission models first simulate a temperature and precipitation distribution over the Northern Hemisphere (e.g. Hopcroft et al., 2013), which allows a direct comparison or calibration of the Greenland temperature simulated in the model to NGRIP temperature increases (Kindler et al., 2013).

ΔCH_4 and ΔT are calculated using splined approximations to the CH_4 data and the temperature reconstruction (Kindler et al., 2013) with cut-off periods of 100 yr. We define empirical thresholds of 0.5 ppbv decade^{-1} and 0.05 °C decade^{-1} in the first derivative of the splines as criteria for the start and end points of the fast increases for every onset of a DO event. The amplitude is then calculated in between these two points. Peaks associated with main events or between main events (see Fig. 1) are named as p16, p17, p18, p23, and p24 and are always preceding the main event with the indicated number. Note that due to problems in the definition of the spline, the start points of the increases in CH_4 were set manually for the DO events 19 and 21. The DO events 2 and 25 were excluded from the calculation due to problems in the attribution of the peaks. The results for ΔCH_4, ΔT, and μ for all the other DO events are summarised in Table 2.

Figure 3 shows that the relation between ΔT and ΔCH_4 is not linear. Huber et al. (2006) report different sensitivity states for the DO events 9–12 compared to the DO events 15–17. Here we find the sensitivity to vary between ~ 5 and ~ 18 ppbv °C^{-1} for all the DO events throughout the last glacial period. The sensitivity of the transition

CPD
9, 4655–4704, 2013

from the Younger Dryas to the Preboreal Holocene (YD/PB) is with $\sim 25.5\,\mathrm{ppbv}\,^{\circ}\mathrm{C}^{-1}$ outstandingly high. Apart from YD/PB, highest sensitivities are found for the DO event 21 and p23, which occurred relatively early during the last glacial. In contrast, the minimum sensitivity is found for DO event 3, which occurred relatively late during the last glacial. However, also DO event 19 and p18 show similarly low sensitivities as DO event 3. The variations in μ are discussed in Sect. 4.2.

3.3 Timing of CH_4 and $\delta^{15}N$

Methane and the stable water isotope records from Greenland revealed unambiguously that there is a close relationship between northern temperature and CH_4 at the onset of DO events. But what is the exact timing of the fast temperature and the CH_4 increases? Due to the age difference of the ice and the gas in a certain depth (Δage), it is difficult to determine a lead or a lag based on a temperature proxy in the ice phase (water isotopes) and a direct atmospheric parameter stored in the air enclosures in the ice (CH_4). Here, we use the gas phase temperature proxy from stable nitrogen isotopes $\delta^{15}N$ to investigate the timing of the fast temperature and CH_4 increases (Severinghaus et al., 1998). This precludes any uncertainty associated with gas age/ice age differences.

For both, the $\delta^{15}N$ and the CH_4 record, we define the onset of a DO event by the two neighboring data points in between which the first significant increase is visible (see example for DO event 5 in Fig. 4). For both gas proxies, the start of the increase is assumed to be between the ages of the two selected time points ($t_{CH_4,old}$, $t_{CH_4,young}$ for CH_4, $t_{\delta^{15}N,old}$, $t_{\delta^{15}N,young}$ for $\delta^{15}N$), with equal probabilities for all ages within this range. The range of possible lags of CH_4 compared to temperature is then constrained by the two age differences:

$$\mathrm{lag}_{min} = t_{\delta^{15}N,young} - t_{CH_4,old}, \quad (2)$$

$$\mathrm{lag}_{max} = t_{\delta^{15}N,old} - t_{CH_4,young}. \quad (3)$$

CPD
9, 4655–4704, 2013

The rate of increase between the selected points is always higher than 1.5 ppbv decade^{-1} for CH_4 and 0.0018 permil decade^{-1} for $\delta^{15}N$. For CH_4, we consider as significant increase if the concentration difference Δc of the two selected data points is greater than 3σ (i.e. with σ equal to 5.9 ppbv such as deduced from our reproducibility test described in Sect. 2; the same criterion is applied for LGGE measurements over the DO events 18–20 and 23–25). In case of doubt ($2\sigma < \Delta c < 3\sigma$), we involve a third data point, at the expense of a higher uncertainty range of the starting point. This was the case for the YD/PB and the DO events 4, 7, 10, 19, 23, and 24. For $\delta^{15}N$ we use a weaker criterion assuming significant increases if one data point is outside of the uncertainty range of the other data point, because the uncertainty is currently set to 0.02 ‰ (Huber et al., 2006), which is a rather conservative estimate. Again, in case of doubt, a third data point is taken into account. This was the case for YD/PB and the DO events 16, and 18. The DO events 2, 3, 22, and 25, as well as p23 and p24, are excluded from the calculations either due to problems in the attribution of the peaks (very low amplitude) or due to a noisy baseline before the event.

We find significant lags of the CH_4 increases compared to temperature increases for the DO events 5, 9, 10, 11, 13, 15, 19, 20, and p18 (see red curve in Fig. 5 for a cumulative probability density function – pdf). For the remaining events, namely for the YD/PB, the BA, and the DO events 4, 6, 7, 8, 12, 14, 16, 17, 18, 21, 23, 24, as well as the peaks p16 and p17, a zero lag is within the equally distributed range of estimated lags (see black curve in Fig. 5). The results are summarised in Table 3. Note that the symmetric shape of the pdf for the phase relationship for all DO events comes about by our conservative lead/lag estimate. In particular we assume that the true onset of the temperature and CH_4 increase lies anywhere between the two samples defining the respective onsets. If we instead just count the DO events for which the last CH_4 sample with stadial concentration precedes the last sample with stadial temperature in $\delta^{15}N$, then this takes place in 4 out of all 25 cases. Accordingly, a lag of CH_4 relative to temperature is more likely than vice versa. We can not exclude a small lead of the CH_4 increase for most of the DO events, but there exists a clear tendency to lags, with

CPD
9, 4655–4704, 2013

a mean value of 56 ± 19 yr over all DO events (expected value and standard error of the mean from brown curve in Fig. 5).

Note that using $\delta^{15}N$ data to investigate the timing of Greenland temperature and CH_4 is not straightforward. First, there is a difference in the gas diffusion constants of CH_4 and nitrogen in the firn column. Buizert et al. (2012) (Supplement) specify values for the relative diffusion constants for the NEEM site of 1.367 for CH_4 and 1.275 for nitrogen relative to the diffusion constant of carbon dioxide (CO_2). This implies that CH_4 diffuses 7 % faster than nitrogen, in agreement with Severinghaus et al. (1998). However, since the time of the gas to diffuse through the total firn column is only about 10 yr (Schwander et al., 1993), the difference in the diffusion constant will cause an offset in the order of only 1–3 yr at the very start of the DO event increase and is negligible compared to the uncertainty of the leads and lags we observe. Second, heat conduction in the firn column causes the thermal gradient between the surface and the close-off depth to vanish after a certain time, which is equivalent to the stabilisation of the $\delta^{15}N$ level at the amount of its gravitational component. However, the thermal conduction in the firn is about 10 times slower than the diffusion of gas. We thus assume that this effect has no influence on the shape of the $\delta^{15}N$ signal at the very start of the increase. Third, the $\delta^{15}N$ is influenced by the diffusive column height and thus by its gravitational enrichment. Apart from temperature, the diffusive column height is influenced by the accumulation rate of the site (Herron and Langway, 1980). A significant increase in the accumulation rate some hundreds of years before the increase in temperature would increase the diffusive column height and thus increase the gravitational part of $\delta^{15}N$ without any change in the temperature. However, on the example of DO event 8, Thomas et al. (2009) showed that the increase in accumulation rate occurs just 2 yr earlier with respect to temperature. Based on their results, we assume that the Greenland accumulation rate and temperature increase occur within a few years for all the DO events, which we consider a reasonable first order approximation.

CPD
9, 4655–4704, 2013

3.4 Interpolar difference at 80–60 kyr BP

The 163 new NGRIP measurements from LGGE Grenoble have been analysed together with the samples from the Antarctic Vostok ice core (Bender et al., 2006) within the same measurement campaign and in the same laboratory and cover approximately the same time interval (80–60 kyr BP). This allows us to precisely estimate the interpolar concentration difference (IPD) of CH_4 within this time interval using the same approach as described by Baumgartner et al. (2012). Figure 6 shows that the fast increases of the DO events 18, 19, and 20 can be identified in both the NGRIP and the Vostok data, which defines tie points for CH_4 synchronisation. However, in between these sharp DO events, no further CH_4 tie points are found. We thus calculate the IPD as a mean over the time interval between two sharp DO event peaks, which yields 20.7 ± 3.0 ppbv (4.6 ± 0.7 %) between DO events 18 and 19 and 19.6 ± 3.7 ppbv (4.4 ± 0.8 %) between DO events 19 and 20, where the numbers in parenthesis are the respective values of the relative interpolar concentration difference (rIPD). Between DO events 17 and 18 the IPD appears to be lower 11.2 ± 5.8 ppbv (2.6 ± 1.4 %) but has a relatively high uncertainty because the NGRIP data from LGGE cover half of the stadial only, which introduces a high synchronisation uncertainty of the first NGRIP data point to the Vostok record. Older than DO event 20, a rIPD reconstruction is not possible since the time resolution of the Vostok record over DO event 21 does not permit a precise synchronisation. Also, we do not estimate a peak interstadial rIPD during the very short lasting DO events 18, 19, and 20, since the attenuation of the atmospheric variation (Spahni et al., 2003) is much stronger in the Vostok ice core compared to the NGRIP ice core. If the NGRIP data are attenuated according to the conditions of the firn at the Vostok site (light blue line in Fig. 6 is the output from the firn model, Schwander et al., 1993; Spahni et al., 2003), the amplitudes of the three DO events are substantially reduced. Estimates of temperature and accumulation rate at the Vostok site between 80–60 kyr BP, which are important parameters in the firn model regarding the gas enclosure process, are taken from Petit et al. (1999) and Siegert (2003). Note

CPD
9, 4655–4704, 2013

that by taking mean IPD values over rather long periods, potential short periods of very low rIPD around 64, 70, and 74 kyr BP might be overlooked. However, two of those appear to have higher IPD values after taking the attenuation into account, while the third example around 70 kyr BP would need additional information on synchronisation to make more detailed statements.

4 Discussion

The discussion focuses on the implication of our results on the evolution of the wetland CH_4 sources over the last glacial cycle. The new NGRIP CH_4 record is compared to CH_4 records from Antarctica in Sect. 4.1 and the variations in the CH_4-to-NGRIP temperature sensitivity μ are discussed in Sect. 4.2. Section 4.3 suggests a potential influence of the atmospheric CO_2 concentration on the wetland CH_4 sources and finally, Sect. 4.4 discusses the timing of CH_4 and NGRIP temperature.

4.1 Information from the interpolar difference

The CH_4 concentrations reconstructed from Greenland and Antarctica are different by some percent, which yields valuable information on the latitudinal distribution of the CH_4 sources (Fig. 7b). Baumgartner et al. (2012) found a relatively stable positive rIPD of about 3–7 % around the LGM (32–11 kyr BP, in green) and revised the zero rIPD estimate from Dällenbach et al. (2000) during the LGM. The rIPD results between 80–60 kyr BP (in green) from the NGRIP and Vostok ice cores presented in this study (Sect. 3.4) show relatively small rIPD in the same order as the values in the stadials before and after DO event 2 from Baumgartner et al. (2012). For the DO events 3–12, Dällenbach et al. (2000) suggested a relative increase of the northern source compared to the southern source from stadial to interstadial based on the rIPD. Here, we merge the existing ice core CH_4 data from EPICA Dronning Maud Land (EDML) (Baumgartner et al., 2012; Capron et al., 2010b; EPICA Community Members, 2006;

CPD
9, 4655–4704, 2013

Schilt et al., 2010b) and Talos Dome Ice Core (TALDICE) (Buiron et al., 2011; Stenni et al., 2011; Schilt et al., 2010b) (red curve in Fig. 7a) and look at the rIPD based on this combined Antarctic record and our new NGRIP record from Greenland (blue curve in Fig. 7a). Very short events, whose amplitudes could have been affected differently by attenuation processes in the different firns (Spahni et al., 2003; Baumgartner et al., 2012), are excluded. In the mean over all DO events, we confirm the statement from Dällenbach et al. (2000) and support a northward shift of the CH_4 sources during the transition from stadial (blue) to interstadial (red) conditions. However, the rIPD as calculated from NGRIP, EDML and TALDICE does not show a continuous reduction over the last glacial cycle as might be expected from the growth of the ice sheets and the associated suppression of the boreal source strength. Note that we refrain from making more detailed statements due to the offsets between the different NGRIP sections (see Sect. 2) and also due to offsets between measurements of Bern and LGGE in the EDML and the TALDICE records. The published records from EDML and TALDICE have been corrected for the 6 ppbv offset between Bern and LGGE (Spahni et al., 2005), however, comparison of all available data reveals remaining mean offsets of another 6.2 ± 1.2 ppbv for TALDICE, and 6.4 ± 1.0 ppbv for EDML for ages younger than 50 kyr BP and 11.9 ± 0.8 ppbv for ages older than 50 kyr BP. We applied these additional offset corrections to bring all values on the Bern reference scale and note that, apart from EDML for ages older than 50 kyr BP, the total offset corrections are well in line with the 12.7 ± 1.1 ppbv offset derived from recently measured NGRIP data at Bern and LGGE over the DO events 23–25 (see Sect. 2). We underline the necessity of analysing in the future both Greenland and Antarctic ice core samples over one single measurement campaign to enable focusing on the rIPD as recently performed by Baumgartner et al. (2012) and in this study over the DO events 18–20 (Sect. 3.4).

4.2 Variations in the CH_4-to-NGRIP temperature sensitivity

The CH_4-to-NGRIP temperature sensitivity μ (Fig. 7c) shows covariation to northern low-latitude summer insolation (Fig. 7d) implying a non-linear response of the increases

CPD
9, 4655–4704, 2013

in CH_4 emissions to temperature increases recorded at the NGRIP site at the onset of DO events. The precessional component visible in μ mainly comes from the CH_4 DO event amplitudes (Fig. 7a), which correlate to tropical or northern mid-latitude summer insolation (Flückiger et al., 2004; Brook et al., 1996). The magnitude of the temperature increases at the NGRIP site itself are not influenced by orbital parameters. Given the local climate dominance on Greenland temperature changes, it is surprising that the connection to northern low-latitude summer insolation is sustained after the inclusion of the NGRIP temperature amplitudes by calculating μ. If we would just randomly choose the NGRIP temperature increase in the range between 8–15 °C (Fig. 3) for each DO event, the connection of μ and northern low-latitude summer insolation would be lost. This may imply that, from one DO event to the other, the relative change in NGRIP temperature amplitude is also representative for the relative temperature change in major parts of the Northern Hemisphere wetland area.

The range of μ (5.0–25.5 ppbv °C^{-1}) obtained from our data compares well to a sensitivity experiment from a wetland CH_4 emission model simulation (6.3–24.1 ppbv °C^{-1}) by Hopcroft et al. (2011), who applied different idealised climate states. Hopcroft et al. (2013) performed a similar experiment for the BA, p17, and the DO events 8 and 11, resulting in sensitivities of 12.2, 11.5, 9.6, and 8.5 ppbv °C^{-1}, respectively. The deviation to our μ values for the specified events is +29, −10, +57, and −41 %, respectively. Hopcroft et al. (2011, 2013) notice that their model generally underestimates the total CH_4 amplitudes, however, it also underestimates the Greenland temperature variations calculated from a fresh-water hosing experiment. The largest deviations are found for the DO event 11 and p17, which occur around extreme northern summer insolation states (Fig. 7d). In comparison, the deviations during the DO event 8 and the BA, which occur during moderate northern summer insolation states, are smaller. Although the different insolation states are taken into account by Hopcroft et al. (2013), it is possible that the influence of northern summer insolation has to be refined in the model.

Based on the connection of CH_4 amplitudes with low-latitude northern summer insolation, Flückiger et al. (2004) concluded that the seasonal distribution of insolation is

CPD
9, 4655–4704, 2013

crucial for wetland CH_4 emission strength at the onset of DO events. The precessional influence is also visible in cave speleothem $\delta^{18}O$ records (Fig. 7g), a proxy for monsoon strength in northern mid-latitudes (Wang et al., 2001, 2008). Apparently, the rapid Greenland DO event temperature variations have counterparts in mid-latitude precipitation records, which implies a far-field influence of extratropical warming on these important CH_4 wetland regions (Chiang and Friedman, 2012). The fast increases in precipitation are in connection with latitudinal shifts of the Intertropical Convergence Zone (ITCZ) and the monsoon systems (Chiang, 2009; Broccoli et al., 2006; Bozbiyik et al., 2011), which moves the necessary amount of moisture from the southern to the CH_4-source rich northern mid-latitudes. Variations in the monsoon strength could drive the non-linear variations in μ via total wetland area and length of emission seasons.

Temperature changes at the onset of DO events reconstructed from NGRIP (Kindler et al., 2013) and used for the calculation of μ reflect changes in mean annual temperatures from stadial to interstadial conditions. In contrast, most important for wetland CH_4 productivity is the averaged temperature at the wetland source location during the warmest months of the year. The amplitude of the seasonal temperature variation, i.e. maximum annual temperature minus mean annual temperature, depends on the amplitude of the seasonal variation in insolation at a given latitude. While the stadial CH_4 baseline does not appear to be strongly modulated by insolation, it is the evolution of the peak interstadial concentration baseline which leads to the covariance of the CH_4 amplitudes and northern summer insolation (Flückiger et al., 2004). Thus the non-linear variations in μ could also be introduced by variations in the difference of maximum annual temperature minus mean annual temperature at mid-latitude wetland source locations during interstadial periods. Note that the peak of μ between 30–40 kyr BP appears to lead the June-July-August (JJA) northern summer insolation by about 5 kyr, while it is in phase with April-May-June (AMJ) northern spring insolation (dashed line in Fig. 7d). This could reflect the contribution of different emission regions in the Northern and Southern Hemisphere, which correlate to different seasonal insolations at their latitudes (Singarayer et al., 2011, Supplement).

CPD
9, 4655–4704, 2013

The transition YD/PB during Termination 1 shows an unusually high CH_4-to-NGRIP temperature sensitivity and belongs, together with the DO events 21, 24, and p17, to the four events with the highest CH_4 amplitudes (Fig. 3). The four events have in common that they are preceded by the four strongest increases visible in the sea level record during the last glacial (Fig. 7h, Rohling et al., 2009; Grant et al., 2012). A strong increase in sea level in a rather short time interval will cause inundation of coastal areas, which were potentially covered by vegetation before. Due to the flooding, the vegetation will die and provide organic material for CH_4 production, leading to the establishment of coastal wetlands. We thus hypothesise that for the YD/PB transition, the DO events 21, 24, and p17, the preceding sea level rise contributed to the very strong CH_4 amplitudes and relatively high μ values within their respective sensitivity state. On longer timescales, however, a higher sea level could also reduce CH_4 emissions since it reduces the total land area (Peltier, 2004). Further, saltier water might mitigate CH_4 emissions through sulfate-reducing bacteria competing with methanogenic archaea (Pester et al., 2012).

From 120 to 20 kyr BP we observe an overall decrease in the maxima and minima of μ, indicated by the dashed regression lines in Fig. 7c. Looking at the insolation curve it is notable that the local maxima in northern summer insolation decrease in parallel to the maxima in μ. Following the argument above, the decrease of the maxima in μ could be a consequence of decreasing wetland extent and/or decreasing summer temperature relative to mean annual temperature at the northern low latitude CH_4 source regions. On the other hand, the local minima in northern summer insolation tend to increase during the glacial, which is not strictly in line with the minima of μ. However, the minimum of μ around 75 kyr BP appears to be lower than the minimum around 45 kyr BP. Southward expansion of the permafrost regions, which would suppress parts of the boreal CH_4 sources, is another reason to expect a decrease in the sensitivity over the last glacial. However, this scenario seems to be inconsistent with our rIPD reconstruction (Fig. 7b), which does not show a continuous reduction over the last glacial as would be expected from a reduced boreal source strength. Another pos-

CPD
9, 4655–4704, 2013

sible candidate which could have a slowly changing influence along with glaciation is the decreasing CO_2 concentration (Fig. 7f, Bereiter et al., 2012; Lüthi et al., 2010; Ahn and Brook, 2007, 2008; Monnin et al., 2001), which is discussed in the next paragraph. In principle, other CH_4 sources than wetlands such as biomass burning could also be responsible for the slow decrease in μ during glaciation, although biomass burning accounts for a rather small fraction of the CH_4 emissions today (Spahni et al., 2011) and biomass burning reductions were not necessarily connected to glacial conditions for all ecosystems (Daniau et al., 2013). Moreover, latest $\delta^{13}CH_4$ measurements over the last glacial cycle show an overall decoupling of CH_4 concentrations and its carbon isotopic signature (Möller et al., 2013) that would be at odds with a major influence of (isotopically heavy) biomass burning emissions on the global CH_4 budget.

4.3 Coupling of CH_4 and CO_2 concentrations

The strength of net primary productivity (NPP) is of central importance for wetland CH_4 emissions, since CH_4 is produced only if organic material is available (Bridgham et al., 2013). Due to the influence of the atmospheric CO_2 concentration on NPP, various bottom-up modelling studies underline the importance of the CO_2 concentration on the CH_4 emission flux. Singarayer et al. (2011) attribute one third of the glacial-interglacial change in the CH_4 concentration to CO_2 effects, either by fertilisation effects or by CO_2 inferred climate change. Melton et al. (2013) also highlight that a high CO_2 concentration facilitates stomatal closure of plants, which reduces the water loss by plants and thus increases the wetland extent. In the most sensitive model, they find a 160 % increase in CH_4 emission flux relative to modern as a result from a stepwise CO_2 increase from 300 to 857 ppmv. Using their modern model CH_4 flux of 264 $Tg\,CH_4\,yr^{-1}$ ($1\,Tg \,\widehat{=}\, 10^{12}\,g$) the 160 % increase translates to 428 $Tg\,CH_4\,yr^{-1}$, which is equal to an increase in the CH_4 flux of 0.8 $Tg\,CH_4\,yr^{-1}$ per ppmv of CO_2. Using a conversion factor from mass to concentration of 2.91 $Tg\,CH_4\,ppbv^{-1}$ (Steele et al., 1992) and solving the steady state mass balance equation with a mean atmospheric lifetime for CH_4 of 8.7 yr

CPD
9, 4655–4704, 2013

(Denman et al., 2007) leads to a sensitivity of 2.3 ppbv CH_4 (ppmv CO_2)$^{-1}$. Accordingly, a maximum effect of 156 ppbv would be expected for the CO_2 decrease from the early glacial (260 ppmv) to the late glacial (200 ppmv) (see Fig. 7f).

Figure 8 shows a comparison of the CH_4 concentration from NGRIP and the CO_2 concentration from various ice cores (Bereiter et al., 2012; Lüthi et al., 2010; Ahn and Brook, 2007, 2008; Monnin et al., 2001) during stadial and interstadial periods. When plotting CH_4 against CO_2 it must be kept in mind that the fast increases in CH_4 concentrations are clearly not driven by the CO_2 concentration. The focus here lies on comparing mean stadial and interstadial levels of CH_4 and CO_2. We attribute to each stadial and interstadial NGRIP CH_4 value a CO_2 concentration, which is calculated by interpolation of the composite CO_2 record to the age of the CH_4 data point. The data points are grouped according to ages younger or older than 70 kyr BP, which corresponds to the age of the MIS5–4 transition observed in the CO_2 data (Fig. 7f). There exists a relatively good correlation for ages younger than 70 kyr BP, especially for interstadial concentrations. We find a sensitivity of 4.3 ppbv CH_4 (ppmv CO_2)$^{-1}$ for interstadial and 2.3 ppbv CH_4 (ppmv CO_2)$^{-1}$ for stadial conditions, which is higher than the minimum and maximum slopes from the different models for modern conditions (Melton et al., 2013) indicated with the purple dashed lines in Fig. 8. Note that the sensitivity to CO_2 changes also depends on the absolute level of CO_2. Vegetation and CH_4 production fertilization by CO_2 is today ($\sim$ 400 ppmv of CO_2) most certainly closer to saturation than during the last glacial period ($\sim$ 200 ppmv of CO_2). From Fig. 8 it becomes clear that although the CO_2 concentration is not the driver of the fast CH_4 increases, it still could be a limiting factor for the amplitudes of these increases. In this view, CO_2 could be seen as a reason for the slowly decreasing μ values by suppression of the CH_4 source strength during the last glacial described in Sect. 4.2.

The parallel evolutions of CH_4 and CO_2 concentrations can also be illustrated on the specific time periods before the DO events 8, 12, and, 17, which are preceded by a slow increase in the CH_4 concentration before the fast CH_4 increase (Fig. 9). At the same time a slow CO_2 increase is visible in line with the major Antarctic Isotope

CPD
9, 4655–4704, 2013

Maximum (AIM) events (Bereiter et al., 2012). Comparing the magnitude of these slow CH_4 and CO_2 increases reveals a sensitivity of 3–5 ppbv CH_4 (ppmv CO_2)$^{-1}$, which is in the same order as in Fig. 8. As mentioned in Sect. 3.1, the DO events 8 and 12 are also preceded by a slow northern temperature increase (see Fig. 1) of about 2–3 °C. Assuming a 50 ppbv increase in CH_4 over these periods (Fig. 9) implies a CH_4-to-NGRIP temperature sensitivity of 17–25 ppbv °C^{-1}, which is relatively high compared to the μ values at the fast increases of DO events 8 and 12. Therefore, it seems unlikely that the magnitude of the slow CH_4 increases can be explained by temperature alone, which would support a direct influence of the increasing CO_2 concentration by increasing biomass production or by increasing wetland extent. A further very prominent example of coinciding slow CH_4 and CO_2 increases is found before the onset of the BA period. In contrast to the DO events 8 and 12, the early increase is not visible in NGRIP temperature (Fig. 1). The 120 ppbv increase in CH_4 corresponds to 40 ppmv in CO_2, which is 3 ppbv CH_4 (ppmv CO_2)$^{-1}$ and thus about the same as in Fig. 9 for the DO events 8, 12, and 17. Similarly, the gradual decreases of CH_4 in the interstadials 12, 14, and in the DO event group 15–17 are accompanied by decreasing CO_2 concentrations. The similar magnitudes for the different intervals strongly suggests an influence of the CO_2 concentration on the stadial/interstadial CH_4 concentration baseline during MIS3–2. Earlier than MIS3, the connection seems to be less apparent. Especially in the transition from MIS5 to MIS4, where a pronounced decrease is visible in CO_2, no corresponding response in the CH_4 concentration is found. This may either imply that the effect is overcompensated by other processes (e.g. Sunda Shelf exposure due to drop in sea level) or that the CH_4 production was limited by other factors than CO_2 during MIS5.

4.4 Timing of CH_4 and NGRIP temperature

Figure 7e shows the timing of the fast NGRIP temperature and CH_4 increases for all considered DO events, with the events showing a significant lag displayed in red. Our

CPD
9, 4655–4704, 2013

reconstruction for DO event 21 is consistent with Vallelonga et al. (2012), who also used the gas phase temperature proxy $\delta^{15}N$ to compare with high-resolution CH_4 data on NGRIP ice and estimate a maximum lag for this event of 69 ± 5 yr with a most probable lag of only a few decades. The processes which could lead to a lag of the CH_4 increases compared to NGRIP temperature increases at the onset of DO events are not well understood. One can think of two extreme CH_4 source evolution scenarios leading to a lag of CH_4. In the first case, where the stadial CH_4 sources are maintained after the start of Greenland warming, all the important additional CH_4 sources causing the stadial-interstadial concentration increase must be delayed by at least the time of the corresponding lag. Otherwise, if there were any important additional sources showing an immediate response to Greenland warming, we would expect the CH_4 concentration to achieve at least parts of its DO event increase instantenously. In the second case a breakdown of parts of the stadial CH_4 sources immediately after the Greenland warming leads to the reduction in emissions compensated by the immediate response of the new sources. Due to the short atmospheric lifetime of CH_4, this process of source compensation could potentially pretend a lag of the CH_4 response to northern warming. In the following we will discuss why we think the second scenario is more likely.

Modelling studies suggest an immediate increase in Northern Hemisphere temperature as a reaction to high-latitude northern warming (e.g. Menviel et al., 2011; Renold et al., 2010). Accordingly, an immediate response of the existing CH_4 wetland source regions would be expected in agreement with the majority of the DO events (Fig. 7e, black). Also an immediate response of boreal wetland CH_4 sources to a rapid cooling is supported in a North Atlantic freshwater hosing experiment by a dynamic vegetation model study (Zürcher et al., 2013). A recent global CH_4 wetland emission model study simulates slightly different temporal evolutions of tropical compared to boreal wetland CH_4 source responses to a DO event warming (Ringeval et al., 2013), but the global increase starts when the first source increases, which is at the same time as the Greenland temperature increase in the same model run (Hopcroft et al., 2011).

CPD
9, 4655–4704, 2013

On the other hand, the concept of latitudinal shifts in the position of the ITCZ at stadial-interstadial transitions (e.g. Bozbiyik et al., 2011; Chiang, 2009; Chiang and Friedman, 2012; Chiang et al., 2003; Wang et al., 2004), which is visible in the speleothem records (Fig. 7g, Wang et al., 2001, 2008), supports a replacement of the stadial by new interstadial CH_4 source regions by displacing the precipitation belts important for the existence of wetlands. Although a comparison of the timing of Greenland temperature and change in tropical moisture is not possible due to relative dating uncertainties between ice core and speleothem records, deuterium excess measurements along the NGRIP ice core for the BA and YD/PB show rapid shifts within a few years, pointing to very fast reorganisation of the atmospheric circulation (Steffensen et al., 2008). In agreement, modelling studies suggest an immediate increase in tropical precipitation as a reaction to high-latitude northern warming (Menviel et al., 2011; Renold et al., 2010), which implies that the lag in the CH_4 increase is probably not due to the time needed to rearrange the global precipitation pattern. A northward shift of the CH_4 sources is also supported by our rIPD reconstruction (Fig. 7b) for most of the DO events. Based on the rIPD a particularly strong northward shift is expected for the DO events 10–11, which are two of those events showing a significant lag compared to NGRIP temperature. The two-box model from Baumgartner et al. (2012) indeed predicts a $\sim 50\,\%$ decrease in the southern hemispheric source strength from stadial to interstadial for such a rIPD configuration, which requires compensation by new source regions before the fast DO event increase of the CH_4 concentrations can start. Looking at CH_4 increase rates, Chappellaz et al. (2013) find maximum increase rates for DO events during the last glacial of 0.6–2.5 ppbv yr^{-1} based on CH_4 measurements from continuous flow analysis along the NEEM ice core. In line with the theory of source compensation, the events showing a significant lag belong to the group of smaller increase rates. It is further apparent that, with the exception of DO event 15, the CH_4 amplitudes of the events showing a lag are relatively small, which means that the orbital configuration was favorable for southern hemispheric emissions before the onset of the DO event (Flückiger et al., 2004). Loosing the southern emissions due to north-

CPD
9, 4655–4704, 2013

ern warming by drastic source replacement could contribute to the very low amplitudes. A drastic replacement of stadial CH_4 sources could further explain a lag of CH_4 by the time needed to transform existing vegetation to wetlands at the new source locations and also to thaw permafrost at high boreal regions. In this context one might argue that a high lag of CH_4 compared to Greenland temperature implies a more drastic latitudinal dislocation of the CH_4 source regions and unfavorable conditions for CH_4 emissions in the Southern Hemisphere.

Comparison of the CH_4/temperature lags with CO_2 data (Fig. 7f, Bereiter et al., 2012) reveals that lags in the CH_4 concentration tend to appear with DO events occurring at relatively low CO_2 concentrations. Note that the variations in CO_2 are closely linked to Antarctic temperature (Bereiter et al., 2012), implying high concentration of CO_2 at the approximate time of the major AIM events (also called A events). The DO events 5, 9, 10, 11, 13, and 15, which show significant lags in the CH_4 increase compared to northern temperature all occur in between major AIM events (CO_2 minima). Conversely, YD/PB, the BA, and the DO events 8, 12, 14, 16, 17, 21, 23, and 24, which occur around major AIM events (CO_2 maxima), tend to show smaller lags around zero in the CH_4 concentration compared to northern temperature. The temperature of the Southern Hemisphere could potentially influence the atmospheric circulation pattern by determining the degree of northward ITCZ shifts at the onset of DO events. Chiang and Friedman (2012) point out the influence of interhemispheric sea surface temperature gradients on tropical rainfall. Changes in AMOC strength related to millennial scale climate variability influence sea surface temperature gradients (Wang et al., 2004). Very cold Antarctic temperatures might shift the ITCZ to more northern latitudes, since the mean position of the ITCZ is biased to the warmer hemisphere (Chiang et al., 2003). A more drastic northward displacement of the CH_4 source for events showing a lag would be in line with the discussion before. A direct influence of the CO_2 concentration on the timing of the fast interstadial temperature and CH_4 increases seems unlikely, especially because the CO_2 concentration variations associated with major AIM events are relatively small (20–40 ppmv, Bereiter et al., 2012).

CPD
9, 4655–4704, 2013

5 Conclusions

We have presented new high resolution CH_4 measurements, which complete and extend the NGRIP record from Termination 1 back to the end of the last interglacial period. We related the amplitudes of the CH_4 increases at the onset of DO events to a temperature record measured along the same ice core (Kindler et al., 2013). The CH_4-to-NGRIP temperature sensitivity shows variations between 5–18 ppbv $^{\circ}C^{-1}$ along with the precessional cycle likely due to variations in temperature or wetland extent at the northern low latitude source regions, and additional modulation of CH_4 source strength by atmospheric CO_2. Calculation of the timing of CH_4 and NGRIP temperature, where we used the $\delta^{15}N$ data of N_2 for temperature (Kindler et al., 2013; Huber et al., 2006; Landais et al., 2004, 2005; Capron et al., 2010a, b, 2012), revealed a tendency to lags of the CH_4 increases of about 56 ± 19 yr on average. We hypothesise that the DO events showing a higher lag are characterised by stronger northward shifts of the source regions, in line with colder Southern Hemisphere temperature causing a stronger northward displacement of the ITCZ. Bottom-up emissions models, which incorporate the processes of ITCZ shifts and transformation from vegetation to wetland area, might be able to simulate the temporal evolution of CH_4 emissions at a DO event transition. We showed that the relative interpolar concentration difference of methane, which is a further important constraint for modelling studies, is 4.6 ± 0.7 % between the DO events 18 and 19 and 4.4 ± 0.8 % between the DO events 19 to 20, which compares well with the rIPD before and after DO event 2 (Baumgartner et al., 2012). With future bipolar measurements over the DO events 5–17, and the DO events 21–25, a reliable rIPD record will be available throughout the last glacial.

Supplementary material related to this article is available online at http://www.clim-past-discuss.net/9/4655/2013/cpd-9-4655-2013-supplement.zip.

CPD
9, 4655–4704, 2013

Acknowledgements. This work, which is a contribution to the North Greenland Ice Core Project (NGRIP), was supported by the University of Bern, the Swiss National Science Foundation, and the Prince Albert II of Monaco Foundation. Additional support was provided by the LEFE programme of CNRS/INSU. NGRIP is coordinated by the Department of Geophysics at the Niels Bohr Institute for Astronomy, Physics and Geophysics, University of Copenhagen. It is supported by Funding Agencies in Denmark (SHF), Belgium (FNRS-CFB), France (IPEV and INSU/CNRS), Germany (AWI), Iceland (RannIs), Japan (MEXT), Sweden (SPRS), Switzerland (SNF) and the United States of America (NSF, Office of Polar Programs). This is Past4Future contribution no xx. The research leading to these results has received funding from the European Union's Seventh Framework programme (FP7/2007–2013) under grant agreement no 243908, Past4Future. Climate change – Learning from the past climate.

References

Ahn, J. and Brook, E. J.: Atmospheric CO_2 and climate from 65 to 30 ka BP, Geophys. Res. Lett., 34, L10703, doi:10.1029/2007GL029551, 2007. 4675, 4676, 4702, 4703, 4704

Ahn, J. and Brook, E. J.: Atmospheric CO_2 and climate on millennial time scales during the last glacial period, Science, 322, 83–85, doi:10.1126/science.1160832, 2008. 4675, 4676, 4702, 4703, 4704

Andersen, K. K., Svensson, A., Johnsen, S. J., Rasmussen, S. O., Bigler, M., Röthlisberger, R., Ruth, U., Siggaard-Andersen, M.-L., Steffensen, J. P., Dahl-Jensen, D., Vinther, B. M., and Clausen, H. B.: The Greenland ice core chronology 2005, 15–42 ka, Part 1: Constructing the time scale, Quaternary Sci. Rev., 25, 3246–3257, doi:10.1016/j.quascirev.2006.08.002, 2006. 4695, 4702

Baumgartner, M., Schilt, A., Eicher, O., Schmitt, J., Schwander, J., Spahni, R., Fischer, H., and Stocker, T. F.: High-resolution interpolar difference of atmospheric methane around the Last Glacial Maximum, Biogeosciences, 9, 3961–3977, doi:10.5194/bg-9-3961-2012, 2012. 4659, 4661, 4662, 4669, 4670, 4671, 4679, 4681, 4695, 4702

Bender, M. L., Floch, G., Chappellaz, J., Suwa, M., Barnola, J.-M., Blunier, T., Dreyfus, G., Jouzel, J., and Parrenin, F.: Gas age–ice age differences and the chronology of the Vostok ice core, 0–100 ka, J. Geophys. Res., 111, D21115, doi:10.1029/2005JD006488, 2006. 4661, 4669, 4700

CPD
9, 4655–4704, 2013

Bereiter, B., Lüthi, D., Siegrist, M., Schüpbach, S., Stocker, T. F., and Fischer, H.: Mode change of millennial CO_2 variability during the last glacial cycle associated with a bipolar marine carbon seesaw, P. Natl. Acad. Sci. USA, 109, 9755–9760, doi:10.1073/pnas.1204069109, 2012. 4675, 4676, 4677, 4680, 4702, 4703, 4704

Bloom, A. A., Palmer, P. I., Fraser, A., Reay, D. S., and Frankenberg, C.: Large-scale controls of methanogenesis inferred from methane and gravity spaceborne data, Science, 327, 322–325, doi:10.1126/science.1175176, 2010. 4658

Boyle, E. A.: Cool tropical temperatures shift the global δ^{18}O-T relationship: an explanation for the ice core δ^{18}O-borehole thermometry conflict?, Geophys. Res. Lett., 24, 273–276, doi:10.1029/97GL00081, 1997. 4659

Bozbiyik, A., Steinacher, M., Joos, F., Stocker, T. F., and Menviel, L.: Fingerprints of changes in the terrestrial carbon cycle in response to large reorganizations in ocean circulation, Clim. Past, 7, 319–338, doi:10.5194/cp-7-319-2011, 2011. 4673, 4679

Bridgham, S. D., Cadillo-Quiroz, H., Keller, J. K., and Zhuang, Q.: Methane emissions from wetlands: biogeochemical, microbial, and modeling perspectives from local to global scales, Global Change Biol., 19, 1325–1346, doi:10.1111/gcb.12131, 2013. 4658, 4675

Broccoli, A. J., Dahl, K. A., and Stouffer, R. J.: Response of the ITCZ to Northern Hemisphere cooling, Geophys. Res. Lett., 33, L01702, doi:10.1029/2005GL024546, 2006. 4673

Brook, E., Sowers, T., and Orchardo, J.: Rapid variations in atmospheric methane concentration during the past 110 000 years, Science, 273, 1087–1091, doi:10.1126/science.273.5278.1087, 1996. 4659, 4672

Brook, E. J., Harder, S., Severinghaus, J., Steig, E. J., and Sucher, C. M.: On the origin and timing of rapid changes in atmospheric methane during the last glacial period, Global Biogeochem. Cy., 14, 559–572, doi:10.1029/1999GB001182, 2000. 4659

Buiron, D., Chappellaz, J., Stenni, B., Frezzotti, M., Baumgartner, M., Capron, E., Landais, A., Lemieux-Dudon, B., Masson-Delmotte, V., Montagnat, M., Parrenin, F., and Schilt, A.: TALDICE-1 age scale of the Talos Dome deep ice core, East Antarctica, Clim. Past, 7, 1–16, doi:10.5194/cp-7-1-2011, 2011. 4671, 4702

Buizert, C., Martinerie, P., Petrenko, V. V., Severinghaus, J. P., Trudinger, C. M., Witrant, E., Rosen, J. L., Orsi, A. J., Rubino, M., Etheridge, D. M., Steele, L. P., Hogan, C., Laube, J. C., Sturges, W. T., Levchenko, V. A., Smith, A. M., Levin, I., Conway, T. J., Dlugokencky, E. J., Lang, P. M., Kawamura, K., Jenk, T. M., White, J. W. C., Sowers, T., Schwander, J., and Blunier, T.: Gas transport in firn: multiple-tracer characterisation and model intercomparison

CPD
9, 4655–4704, 2013

for NEEM, Northern Greenland, Atmos. Chem. Phys., 12, 4259–4277, doi:10.5194/acp-12-4259-2012, 2012. 4668

Capron, E., Landais, A., Chappellaz, J., Schilt, A., Buiron, D., Dahl-Jensen, D., Johnsen, S. J., Jouzel, J., Lemieux-Dudon, B., Loulergue, L., Leuenberger, M., Masson-Delmotte, V., Meyer, H., Oerter, H., and Stenni, B.: Millennial and sub-millennial scale climatic variations recorded in polar ice cores over the last glacial period, Clim. Past, 6, 345–365, doi:10.5194/cp-6-345-2010, 2010a. 4660, 4681, 4695

Capron, E., Landais, A., Lemieux-Dudon, B., Schilt, A., Masson-Delmotte, V., Buiron, D., Chappellaz, J., Dahl-Jensen, D., Johnsen, S., Leuenberger, M., Loulergue, L., and Oerter, H.: Synchronising EDML and NorthGRIP ice cores using $\delta^{18}O$ of atmospheric oxygen ($\delta^{18}O$ (atm)) and CH_4 measurements over MIS5 (80–123 kyr), Quaternary Sci. Rev., 29, 222–234, doi:10.1016/j.quascirev.2009.07.014, 2010b. 4660, 4661, 4662, 4670, 4681, 4692, 4695, 4702

Capron, E., Landais, A., Chappellaz, J., Buiron, D., Fischer, H., Johnsen, S. J., Jouzel, J., Leuenberger, M., Masson-Delmotte, V., and Stocker, T. F.: A global picture of the first abrupt climatic event occurring during the last glacial inception, Geophys. Res. Lett., 39, L15703, doi:10.1029/2012GL052656, 2012. 4660, 4661, 4662, 4681, 4692, 4695, 4702

Chappellaz, J., Blunier, T., Kints, S., Dällenbach, A., Barnola, J. M., Schwander, J., Raynaud, D., and Stauffer, B.: Changes in the atmospheric CH_4 gradient between Greenland and Antarctica during the Holocene, J. Geophys. Res.-Atmos., 102, 15987–15997, 1997. 4659, 4660, 4661

Chappellaz, J., Stowasser, C., Blunier, T., Baslev-Clausen, D., Brook, E.J., Dallmayr, R., Faïn, X., Lee, J.E., Mitchell, L.E., Pascual, O., Romanini, D., Rosen, J., and Schüpbach, S.: High-resolution glacial and deglacial record of atmospheric methane by continuous-flow and laser spectrometer analysis along the NEEM ice core, Clim. Past Discuss., 9, 2517–2556, doi:10.5194/cpd-9-2517-2013, 2013. 4658, 4663, 4664, 4679

Chiang, J. C.: The tropics in Paleoclimate, Annu. Rev. Earth Pl. Sc., 37, 263–297, doi:10.1146/annurev.earth.031208.100217, 2009. 4673, 4679

Chiang, J. C. and Friedman, A. R.: Extratropical cooling, interhemispheric thermal gradients, and tropical climate change, Annu. Rev. Earth Pl. Sc., 40, 383–412, doi:10.1146/annurev-earth-042711-105545, 2012. 4673, 4679, 4680

CPD
9, 4655–4704, 2013

Chiang, J. C. H., Biasutti, M., and Battisti, D.: Sensitivity of the Atlantic Intertropical Convergence Zone to Last Glacial Maximum boundary conditions, Paleoceanography, 18, 1094, doi:10.1029/2003PA000916, 2003. 4679, 4680

Christensen, T. R., Ekberg, A., Ström, L., Mastepanov, M., Panikov, N., Öquist, M., Svensson, B. H., Nykänen, H., Martikainen, P. J., and Oskarsson, H.: Factors controlling large scale variations in methane emissions from wetlands, Geophys. Res. Lett., 30, 1414, doi:10.1029/2002GL016848, 2003. 4658

Clement, A. C. and Peterson, L. C.: Mechanisms of abrupt climate change of the last glacial period, Rev. Geophys., 46, RG4002, doi:10.1029/2006RG000204, 2008. 4659

Dällenbach, A., Blunier, T., Flückiger, J., Stauffer, B., Chappellaz, J., and Raynaud, D.: Changes in the atmospheric CH_4 gradient between Greenland and Antarctica during the Last Glacial and the transition to the Holocene, Geophys. Res. Lett., 27, 1005–1008, 2000. 4670, 4671

Daniau, A.-L., Sánchez Goñi, M. F., Martinez, P., Urrego, D. H., Bout-Roumazeilles, V., Desprat, S., and Marlon, J. R.: Orbital-scale climate forcing of grassland burning in southern Africa, P. Natl. Acad. Sci. USA, 110, 5069–5073, doi:10.1073/pnas.1214292110, 2013. 4675

Dansgaard, W., Clausen, H. B., Gundestrup, N., Hammer, C. U., Johnsen, S. F., Kristinsdottir, P. M., and Reeh, N.: A new Greenland deep ice core, Science, 218, 1273–1277, doi:10.1126/science.218.4579.1273, 1982. 4659

Denman, K., Brasseur, G., Chidthaisong, A., Ciais, P., Cox, P., Dickinson, R., Hauglustaine, D., Heinze, C., Holland, E., Jacob, D., Lohmann, U., Ramachandran, D., da Silva Dias, P., Wofsy, S., and Zhang, X.: Couplings Between Changes in the Climate System and Biogeochemistry, Climate Change 2007: The Physical Science Basis, Contribution of Working Group I to the Fourth Assessment Report of the Intergovernmental Panel on Climate Change, Cambridge University Press, Cambridge, UK and New York, NY, USA, 2007. 4658, 4676

EPICA Community Members: One-to-one coupling of glacial climate variability in Greenland and Antarctica, Nature, 444, 195–198, 2006. 4670, 4702

Etheridge, D. M., Steele, L. P., Francey, R. J., and Langenfelds, R. L.: Atmospheric methane between 1000 AD and present: evidence of anthropogenic emissions and climatic variability, J. Geophys. Res.-Atmos., 103, 15979–15993, doi:10.1029/98JD00923, 1998. 4658

Flückiger, J., Blunier, T., Stauffer, B., Chappellaz, J., Spahni, R., Kawamura, K., Schwander, J., Stocker, T. F., and Dahl-Jensen, D.: N_2O and CH_4 variations during the last

CPD
9, 4655–4704, 2013

glacial epoch: insight into global processes, Global Biogeochem. Cy., 18, GB1020, doi:10.1029/2003GB002122, 2004. 4660, 4661, 4662, 4672, 4673, 4679, 4692, 4695, 4702
Grant, K. M., Rohling, E. J., Bar-Matthews, M., Ayalon, A., Medina-Elizalde, M., Ramsey, C. B., Satow, C., and Roberts, A. P.: Rapid coupling between ice volume and polar temperature over the past 150 000 years, Nature, 491, 744–747, doi:10.1038/nature11593, 2012. 4674, 4702
Herron, M. M. and Langway, C. C.: Firn densification – an empirical-model, J. Glaciol., 25, 373–385, 1980. 4668
Hopcroft, P. O., Valdes, P. J., and Beerling, D. J.: Simulating idealized Dansgaard–Oeschger events and their potential impacts on the global methane cycle, Quaternary Sci. Rev., 30, 3258–3268, doi:10.1016/j.quascirev.2011.08.012, 2011. 4672, 4678
Hopcroft, P. O., Valdes, P. J., Wania, R., and Beerling, D. J.: Limited response of peatland CH_4 emissions to abrupt Atlantic Ocean circulation changes in glacial climates, Clim. Past Discuss., 9, 3519–3561, doi:10.5194/cpd-9-3519-2013, 2013. 4665, 4672
Huber, C., Leuenberger, M., Spahni, R., Flückiger, J., Schwander, J., Stocker, T. F., Johnsen, S., Landais, A., and Jouzel, J.: Isotope calibrated Greenland temperature record over Marine Isotope Stage 3 and its relation to CH_4, Earth Planet. Sc. Lett., 243, 504–519, 2006. 4659, 4660, 4661, 4662, 4663, 4665, 4667, 4681, 4692, 4695, 4700, 4702
Johnsen, S. J., Dahl-Jensen, D., Gundestrup, N., Steffensen, J. P., Clausen, H., Miller, H., Masson-Delmotte, V., Sveinbjornsdottir, A., and White, J.: Oxygen isotope and palaeotemperature records from six Greenland ice-core stations: Camp Century, Dye-3, GRIP, GISP2, Renland and NorthGRIP, J. Quaternary Sci., 16, 299–307, 2001. 4695, 4702
Kindler, P., Guillevic, M., Baumgartner, M., Schwander, J., Landais, A., and Leuenberger, M.: NGRIP temperature reconstruction from 10 to 120 kyr b2k, Clim. Past Discuss., 9, 4099–4143, doi:10.5194/cpd-9-4099-2013, 2013. 4660, 4663, 4665, 4673, 4681, 4695, 4698, 4702
Krinner, G., Genthon, C., and Jouzel, J.: GCM analysis of local influences on ice core delta signals, Geophys. Res. Lett., 24, 2825–2828, doi:10.1029/97GL52891, 1997. 4659
Landais, A., Barnola, J. M., Masson-Delmotte, V., Jouzel, J., Chappellaz, J., Caillon, N., Huber, C., Leuenberger, M., and Johnsen, S. J.: A continuous record of temperature evolution over a sequence of Dansgaard–Oeschger events during marine isotopic stage 4 (76 to 62 kyr BP), Geophys. Res. Lett., 31, L22211, doi:10.1029/2004GL021193, 2004. 4660, 4681, 4695

CPD
9, 4655–4704, 2013

Landais, A., Jouzel, J., Masson-Delmotte, V., and Caillon, N.: Large temperature variations over rapid climatic events in Greenland: a method based on air isotopic measurements, C. R. Geosci., 337, 947–956, doi:10.1016/j.crte.2005.04.003, 2005. 4660, 4681, 4695

Lang, C., Leuenberger, M., Schwander, J., and Johnsen, S.: 16 °C rapid temperature variation in Central Greenland 70 000 years ago, Science, 286, 934–937, doi:10.1126/science.286.5441.934, 1999. 4659

Levine, J. G., Wolff, E. W., Jones, A. E., Sime, L. C., Valdes, P. J., Archibald, A. T., Carver, G. D., Warwick, N. J., and Pyle, J. A.: Reconciling the changes in atmospheric methane sources and sinks between the Last Glacial Maximum and the pre-industrial era, Geophys. Res. Lett., 38, L23804, doi:10.1029/2011GL049545, 2011. 4658

Levine, J. G., Wolff, E. W., Hopcroft, P. O., and Valdes, P. J.: Controls on the tropospheric oxidizing capacity during an idealized Dansgaard–Oeschger event, and their implications for the rapid rises in atmospheric methane during the last glacial period, Geophys. Res. Lett., 39, L12805, doi:10.1029/2012GL051866, 2012. 4658

Li, C., Battisti, D. S., and Bitz, C. M.: Can North Atlantic sea ice anomalies account for Dansgaard–Oeschger climate signals?, J. Climate, 23, 5457–5475, doi:10.1175/2010JCLI3409.1, 2010. 4659

Loulergue, L., Schilt, A., Spahni, R., Masson-Delmotte, V., Blunier, T., Lemieux, B., Barnola, J.-M., Raynaud, D., Stocker, T. F., and Chappellaz, J.: Orbital and millennial-scale features of atmospheric CH_4 over the past 800 000 years, Nature, 453, 383–386, doi:10.1038/nature06950, 2008. 4657

Lüthi, D., Bereiter, B., Stauffer, B., Winkler, R., Schwander, J., Kindler, P., Leuenberger, M., Kipfstuhl, S., Capron, E., Landais, A., Fischer, H., and Stocker, T. F.: CO_2 and O_2/N_2 variations in and just below the bubble-clathrate transformation zone of Antarctic ice cores, Earth Planet. Sc. Lett., 297, 226–233, doi:10.1016/j.epsl.2010.06.023, 2010. 4675, 4676, 4702, 4703, 4704

Melton, J. R., Wania, R., Hodson, E. L., Poulter, B., Ringeval, B., Spahni, R., Bohn, T., Avis, C. A., Beerling, D. J., Chen, G., Eliseev, A. V., Denisov, S. N., Hopcroft, P. O., Lettenmaier, D. P., Riley, W. J., Singarayer, J. S., Subin, Z. M., Tian, H., Zürcher, S., Brovkin, V., van Bodegom, P. M., Kleinen, T., Yu, Z. C., and Kaplan, J. O.: Present state of global wetland extent and wetland methane modelling: conclusions from a model inter-comparison project (WETCHIMP), Biogeosciences, 10, 753–788, doi:10.5194/bg-10-753-2013, 2013. 4658, 4675, 4676, 4703

CPD
9, 4655–4704, 2013

Menviel, L., Timmermann, A., Timm, O. E., and Mouchet, A.: Deconstructing the Last Glacial termination: the role of millennial and orbital-scale forcings, Quaternary Sci. Rev., 30, 1155–1172, doi:10.1016/j.quascirev.2011.02.005, 2011. 4678, 4679

Möller, L., Sowers, T., Bock, M., Spahni, R., Behrens, M., Schmitt, J., Miller, H., and Fischer, H.: Independent variations of CH_4 emissions and isotopic composition over the past 160 000 years, Nat. Geosci., 0, accepted, 2013. 4675

Monnin, E., Indermühle, A., Dällenbach, A., Flückiger, J., Stauffer, B., Stocker, T. F., Raynaud, D., and Barnola, J.-M.: Atmospheric CO_2 concentrations over the Last Glacial termination, Science, 291, 112–114, doi:10.1126/science.291.5501.112, 2001. 4675, 4676, 4702, 4703, 4704

NGRIP Project Members: High-resolution record of Northern Hemisphere climate extending into the last interglacial period, Nature, 431, 147–151, 2004. 4659, 4695, 4702

Peltier, W.: Global glacial isostasy and the surface of the ice-age Earth: the ICE-5G (VM2) model and GRACE, Annu. Rev. Earth Pl. Sc., 32, 111–149, doi:10.1146/annurev.earth.32.082503.144359, 2004. 4674

Pester, M., Knorr, K. H., Friedrich, M. W., Wagner, M., and Loy, A.: Sulfate-reducing microorganisms in wetlands – fameless actors in carbon cycling and climate change, Front. Microbiol., 3, doi:10.3389/fmicb.2012.00072, in press, 2012. 4674

Petersen, S. V., Schrag, D. P., and Clark, P. U.: A new mechanism for Dansgaard–Oeschger cycles, Paleoceanography, 28, 24–30, doi:10.1029/2012PA002364, 2013. 4659

Petit, J., Jouzel, J., Raynaud, D., Barkov, N., Barnola, J., Basile, I., Bender, M., Chappellaz, J., Davis, M., Delaygue, G., Delmotte, M., Kotlyakov, V., Legrand, M., Lipenkov, V., Lorius, C., Pepin, L., Ritz, C., Saltzman, E., and Stievenard, M.: Climate and atmospheric history of the past 420,000 years from the Vostok ice core, Antarctica, Nature, 399, 429–436, doi:10.1038/20859, 1999. 4669

Quinn, T., Tremaine, S., and Duncan, M.: A 3 million year integration of the Earths orbit, Astron. J., 101, 2287–2305, 1991. 4702

Renold, M., Raible, C. C., Yoshimori, M., and Stocker, T. F.: Simulated resumption of the North Atlantic meridional overturning circulation – slow basin-wide advection and abrupt local convection, Quaternary Sci. Rev., 29, 101–112, doi:10.1016/j.quascirev.2009.11.005, 2010. 4678, 4679

Ringeval, B., Hopcroft, P. O., Valdes, P. J., Ciais, P., Ramstein, G., Dolman, A. J., and Kageyama, M.: Response of methane emissions from wetlands to the Last Glacial Maximum

CPD
9, 4655–4704, 2013

and an idealized Dansgaard–Oeschger climate event: insights from two models of different complexity, Clim. Past, 9, 149–171, doi:10.5194/cp-9-149-2013, 2013. 4658, 4678
Rohling, E. J., Grant, K., Bolshaw, M., Roberts, A. P., Siddall, M., Hemleben, C., and Kucera, M.: Antarctic temperature and global sea level closely coupled over the past five glacial cycles, Nat. Geosci., 2, 500–504, doi:10.1038/ngeo557, 2009. 4674, 4702
Schilt, A., Baumgartner, M., Blunier, T., Schwander, J., Spahni, R., Fischer, H., and Stocker, T. F.: Glacial-interglacial and millennial-scale variations in the atmospheric nitrous oxide concentration during the last 800 000 years, Quaternary Sci. Rev., 29, 182–192, 2010a. 4661
Schilt, A., Baumgartner, M., Schwander, J., Buiron, D., Capron, E., Chappellaz, J., Loulergue, L., Schüpbach, S., Spahni, R., Fischer, H., and Stocker, T. F.: Atmospheric nitrous oxide during the last 140 000 years, Earth Planet. Sc. Lett., 300, 33–43, 2010b. 4661, 4662, 4671, 4692, 4695, 4702
Schwander, J., Barnola, J. M., Andrie, C., Leuenberger, M., Ludin, A., Raynaud, D., and Stauffer, B.: The age of the air in the firn and the ice at Summit, Greenland, J. Geophys. Res.-Atmos., 98, 2831–2838, 1993. 4663, 4668, 4669, 4700
Schwander, J., Sowers, T., Barnola, J., Blunier, T., Fuchs, A., and Malaize, B.: Age scale of the air in the summit ice: implication for glacial-interglacial temperature change, J. Geophys. Res.-Atmos., 102, 19483–19493, doi:10.1029/97JD01309, 1997. 4663
Serreze, M. C. and Barry, R. G.: Processes and impacts of Arctic amplification: a research synthesis, Global Planet. Change, 77, 85–96, doi:10.1016/j.gloplacha.2011.03.004, 2011. 4665
Severinghaus, J. P. and Brook, E. J.: Abrupt climate change at the end of the Last Glacial period inferred from trapped air in Polar ice, Science, 286, 930–934, doi:10.1126/science.286.5441.930, 1999. 4659
Severinghaus, J. P., Sowers, T., Brook, E. J., Alley, R. B., and Bender, M. L.: Timing of abrupt climate change at the end of the Younger Dryas interval from thermally fractionated gases in polar ice, Nature, 391, 141–146, doi:10.1038/34346, 1998. 4659, 4660, 4666, 4668
Siegert, M.: Glacial-interglacial variations in central East Antarctic ice accumulation rates, Quaternary Sci. Rev., 22, 741–750, doi:10.1016/S0277-3791(02)00191-9, 2003. 4669
Singarayer, J. S., Valdes, P. J., Friedlingstein, P., Nelson, S., and Beerling, D. J.: Late Holocene methane rise caused by orbitally controlled increase in tropical sources, Nature, 470, 82–85, 2011. 4673, 4675

CPD
9, 4655–4704, 2013

Spahni, R., Schwander, J., Flückiger, J., Stauffer, B., Chappellaz, J., and Raynaud, D.: The attenuation of fast atmospheric CH_4 variations recorded in polar ice cores, Geophys. Res. Lett., 30, 1571, doi:10.1029/2003GL017093, 2003. 4663, 4669, 4671, 4700

Spahni, R., Chappellaz, J., Stocker, T. F., Loulergue, L., Hausammann, G., Kawamura, K., Flückiger, J., Schwander, J., Raynaud, D., Masson-Delmotte, V., and Jouzel, J.: Atmospheric methane and nitrous oxide of the Late Pleistocene from Antarctic ice cores, Science, 310, 1317–1321, doi:10.1126/science.1120132, 2005. 4661, 4662, 4671

Spahni, R., Wania, R., Neef, L., van Weele, M., Pison, I., Bousquet, P., Frankenberg, C., Foster, P. N., Joos, F., Prentice, I. C., and van Velthoven, P.: Constraining global methane emissions and uptake by ecosystems, Biogeosciences, 8, 1643–1665, doi:10.5194/bg-8-1643-2011, 2011. 4658, 4659, 4675

Steele, L., Dlugokencky, E., Lang, P., Tans, P., Martin, R., and Masarie, K.: Slowing down of the global accumulation of atmospheric methane during the 1980s, Nature, 358, 313–316, 1992. 4675

Steffensen, J. P., Andersen, K. K., Bigler, M., Clausen, H. B., Dahl-Jensen, D., Fischer, H., Goto-Azuma, K., Hansson, M., Johnsen, S. J., Jouzel, J., Masson-Delmotte, V., Popp, T., Rasmussen, S. O., Roethlisberger, R., Ruth, U., Stauffer, B., Siggaard-Andersen, M.-L., Sveinbjornsdottir, A. E., Svensson, A., and White, J. W. C.: High-resolution Greenland ice core data show abrupt climate change happens in few years, Science, 321, 680–684, doi:10.1126/science.1157707, 2008. 4679

Stenni, B., Buiron, D., Frezzotti, M., Albani, S., Barbante, C., Bard, E., Barnola, J. M., Baroni, M., Baumgartner, M., Bonazza, M., Capron, E., Castellano, E., Chappellaz, J., Delmonte, B., Falourd, S., Genoni, L., Iacumin, P., Jouzel, J., Kipfstuhl, S., Landais, A., Lemieux-Dudon, B., Maggi, V., Masson-Delmotte, V., Mazzola, C., Minster, B., Montagnat, M., Mulvaney, R., Narcisi, B., Oerter, H., Parrenin, F., Petit, J. R., Ritz, C., Scarchilli, C., Schilt, A., Schüpbach, S., Schwander, J., Selmo, E., Severi, M., Stocker, T. F., and Udisti, R.: Expression of the bipolar see-saw in Antarctic climate records during the last deglaciation, Nat. Geosci., 4, 46–49, 2011. 4671, 4702

Stocker, T. F. and Johnsen, S. J.: A minimum thermodynamic model for the bipolar seesaw, Paleoceanography, 18, 1087, doi:10.1029/2003PA000920, 2003. 4659

Thomas, E. R., Wolff, E. W., Mulvaney, R., Johnsen, S. J., Steffensen, J. P., and Arrowsmith, C.: Anatomy of a Dansgaard–Oeschger warming transition: high-resolution analy-

CPD
9, 4655–4704, 2013

sis of the North Greenland Ice Core Project ice core, J. Geophys. Res., 114, D08102, doi:10.1029/2008JD011215, 2009. 4668

Vallelonga, P., Bertagna, G., Blunier, T., Kjær, H. A., Popp, T. J., Rasmussen, S. O., Steffensen, J. P., Stowasser, C., Svensson, A. S., Warming, E., Winstrup, M., Bigler, M., and Kipfstuhl, S.: Duration of Greenland Stadial 22 and ice-gas Δage from counting of annual layers in Greenland NGRIP ice core, Clim. Past, 8, 1839–1847, doi:10.5194/cp-8-1839-2012, 2012. 4678

Voelker, A. H.: Global distribution of centennial-scale records for Marine Isotope Stage (MIS) 3: a database, Quaternary Sci. Rev., 21, 1185–1212, doi:10.1016/S0277-3791(01)00139-1, 2002. 4659

Walter, B. P., Heimann, M., and Matthews, E.: Modeling modern methane emissions from natural wetlands: 1. Model description and results, J. Geophys. Res.-Atmos., 106, 34189–34206, doi:10.1029/2001JD900165, 2001. 4658

Wang, X., Auler, A., Edwards, R., Cheng, H., Cristalli, P., Smart, P., Richards, D., and Shen, C.: Wet periods in northeastern Brazil over the past 210 kyr linked to distant climate anomalies, Nature, 432, 740–743, doi:10.1038/nature03067, 2004. 4679, 4680

Wang, Y. J., Cheng, H., Edwards, R. L., An, Z. S., Wu, J. Y., Shen, C. C., and Dorale, J. A.: A high-resolution absolute-dated Late Pleistocene monsoon record from Hulu Cave, China, Science, 294, 2345–2348, 2001. 4673, 4679, 4702

Wang, Y. J., Cheng, H., Edwards, R. L., Kong, X., Shao, X., Chen, S., Wu, J., Jiang, X., Wang, X., and An, Z.: Millennial- and orbital-scale changes in the East Asian monsoon over the past 224 000 years, Nature, 451, 1090–1093, doi:10.1038/nature06692, 2008. 4673, 4679, 4702

Wania, R., Melton, J. R., Hodson, E. L., Poulter, B., Ringeval, B., Spahni, R., Bohn, T., Avis, C. A., Chen, G., Eliseev, A. V., Hopcroft, P. O., Riley, W. J., Subin, Z. M., Tian, H., Brovkin, V., van Bodegom, P. M., Kleinen, T., Yu, Z. C., Singarayer, J. S., Zürcher, S., Lettenmaier, D. P., Beerling, D. J., Denisov, S. N., Prigent, C., Papa, F., and Kaplan, J. O.: Present state of global wetland extent and wetland methane modelling: methodology of a model intercomparison project (WETCHIMP), Geosci. Model Dev. Discuss., 5, 4071–4136, doi:10.5194/gmdd-5-4071-2012, 2012. 4658

Zürcher, S., Spahni, R., Joos, F., Steinacher, M., and Fischer, H.: Impact of an abrupt cooling event on interglacial methane emissions in northern peatlands, Biogeosciences, 10, 1963–1981, doi:10.5194/bg-10-1963-2013, 2013. 4658, 4678

CPD
9, 4655–4704, 2013

Table 1. Concentration offsets of new data measured in Bern during the years 2010–2012 compared to previously measured data along the NGRIP ice core.

Reference study	Climatic period	*n* #	Mean (ppbv)	Median (ppbv)	SD (ppbv)	SE (ppbv)	Year of analysis
Huber et al. (2006)	DO 15–17	41.0	2.9	2.4	12.2	1.9	2004
Schilt et al. (2010b)	T1	31.0	8.4	8.0	16.1	2.9	2002
Flückiger et al. (2004)	DO 9–12	43.0	14.5	15.7	9.3	1.4	2002
Capron et al. (2010b, 2012)	DO 23–25	188.0	12.2	13.0	16.5	1.2	2009–2012
new data LGGE	DO 18–20	153.0	26.5	26.4	12.4	1.0	2001–2002

CPD
9, 4655–4704, 2013

Table 2. Methane amplitude ΔCH_4 (ppbv), temperature amplitude ΔT (°C), and sensitivity (ppbv °C^{-1}) for the fast increases of DO events.

DO	ΔCH_4 (ppbv)	ΔT (°C)	μ (ppbv °C^{-1})
0	260.2	10.2	25.5
1	118.2	12.5	9.4
3	63.8	12.6	5.0
4	91.3	12.3	7.4
5	91.6	12.3	7.5
6	100.4	9.3	10.8
7	155.8	11.2	13.9
8	128.7	10.1	12.8
9	75.9	6.3	12.1
10	95.7	13.5	7.1
11	85.9	14.1	6.1
12	87.4	12.6	6.9
13	63.8	8.3	7.6
14	145.9	12.5	11.6
15	148.1	9.7	15.3
16	92.0	6.6	14.0
p16	116.0	10.0	11.6
17	144.0	10.4	13.8
p17	182.7	12.7	14.4
18	113.5	10.1	11.2
p18	44.8	8.3	5.4
19	69.8	13.9	5.0
20	97.4	12.2	8.0
21	222.1	13.5	16.5
22	50.9	5.3	9.6
23	99.3	9.8	10.1
p23	126.6	7.0	18.1
24	177.0	15.0	11.8
p24	41.6	4.8	8.6

CPD
9, 4655–4704, 2013

Table 3. Depth interval [d_{young}, d_{old}], time interval [t_{young}, t_{old}], and lag interval [lag_{min}, lag_{max}] calculated from Eqs. (2) and (3) at the begin of the fast increases in CH_4 and $\delta^{15}N$ at the onset of DO events.

DO	$d_{CH_4,young}$ (m)	$d_{CH_4,old}$ (m)	$d_{\delta^{15}N,young}$ (m)	$d_{\delta^{15}N,old}$ (m)	$t_{CH_4,young}$ (yr)	$t_{CH_4,old}$ (yr)	$t_{\delta^{15}N,young}$ (yr)	$t_{\delta^{15}N,old}$ (yr)	lag_{min} (yr)	lag_{max} (yr)
0	1518.0	1519.7	1517.5	1519.8	11 533.2	11 585.7	11 519.4	11 589.9	−66	57
1	1631.3	1633.0	1631.4	1634.7	14 653.5	14 711.3	14 657.7	14 778.6	−54	125
4	1912.9	1914.6	1913.6	1915.0	28 572.5	28 682.7	28 611.9	28 714.2	−71	142
5	1974.0	1975.1	1975.5	1976.3	32 309.8	32 422.7	32 465.5	32 555.9	43	246
6	1996.0	1997.1	1995.0	1996.1	33 642.3	33 721.5	33 581.9	33 649.1	−140	7
7	2029.0	2031.2	2029.3	2030.1	35 387.3	35 525.1	35 402.6	35 450.7	−122	63
8	2088.0	2088.4	2087.7	2089.8	38 400.8	38 424.4	38 383.6	38 509.3	−41	109
9	2117.5	2119.2	2119.6	2120.5	40 435.8	40 560.9	40 592.8	40 669.1	32	233
10	2140.6	2142.3	2142.7	2144.6	41 748.9	41 875.3	41 908.1	42 083.5	33	335
11	2173.0	2174.2	2174.5	2176.6	43 654.0	43 730.5	43 754.5	43 972.1	24	318
12	2236.4	2236.9	2236.6	2237.1	47 459.5	47 496.5	47 476.5	47 512.0	−20	52
13	2269.3	2270.4	2270.7	2271.7	49 792.5	49 873.4	49 899.5	49 980.0	26	188
14	2357.9	2358.9	2357.1	2358.2	55 144.4	55 245.3	55 077.7	55 173.2	−168	29
15	2377.7	2378.8	2379.1	2380.2	56 591.9	56 685.3	56 717.0	56 821.2	32	229
16	2410.1	2410.7	2409.9	2411.9	58 815.0	58 859.6	58 802.5	58 943.4	−57	128
p16	2413.4	2414.0	2413.2	2414.2	59 051.2	59 110.1	59 037.0	59 130.2	−73	79
17	2425.5	2426.1	2425.3	2426.3	59 869.5	59 910.4	59 856.6	59 922.5	−54	53
p17	2431.6	2432.7	2431.9	2432.8	60 203.2	60 294.1	60 228.4	60 309.2	−66	106
18	2474.4	2476.1	2474.0	2477.3	64 772.1	64 963.6	64 743.7	65 128.2	−220	356
p18	2515.1	2515.7	2515.8	2516.2	70 277.4	70 356.6	70 368.7	70 442.0	12	165
19	2542.3	2543.7	2543.7	2545.5	72 897.3	73 003.7	73 008.1	73 298.3	4	401
20	2586.1	2586.6	2586.6	2587.3	77 121.8	77 167.1	77 170.9	77 259.6	4	138
21	2692.3	2693.4	2693.3	2693.9	85 365.7	85 429.7	85 428.0	85 468.1	−2	102
23	2896.0	2897.2	2896.9	2897.4	104 696.8	104 820.2	104 783.7	104 849.2	−36	152
24	2945.2	2946.1	2945.3	2945.8	109 121.3	109 245.8	109 130.8	109 209.7	−115	88

CPD
9, 4655–4704, 2013

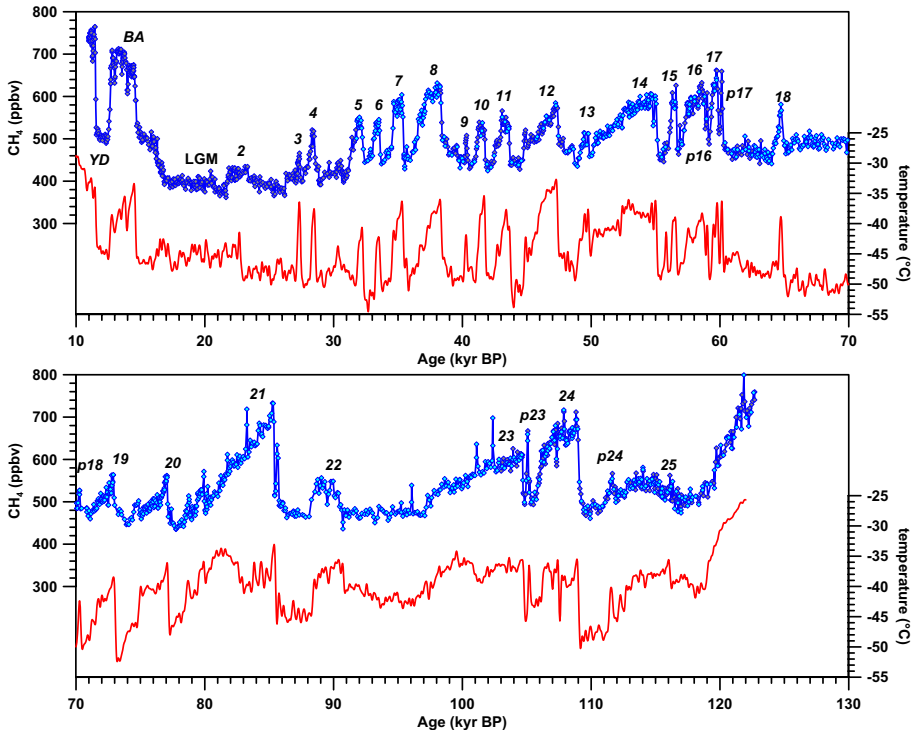

Fig. 1. NGRIP methane and temperature from Termination 1 back to the end of the last interglacial period. Methane concentrations in grey (Baumgartner et al., 2012; Capron et al., 2010b, 2012; Schilt et al., 2010b; Huber et al., 2006; Flückiger et al., 2004) and blue (new data), temperature in red (Kindler et al., 2013). δ^{18}O derived temperature was calibrated by NGRIP δ^{15}N data (Kindler et al., 2013; Huber et al., 2006; Landais et al., 2004, 2005; Capron et al., 2010a, b, 2012). The records are shown on the gas age scale calculated by Kindler et al. (2013) based on the ss09sea06bm ice age scale (NGRIP Project Members, 2004; Andersen et al., 2006; Johnsen et al., 2001). Numbers of DO events are displayed in italics.

CPD
9, 4655–4704, 2013

NGRIP methane record

M. Baumgartner et al.

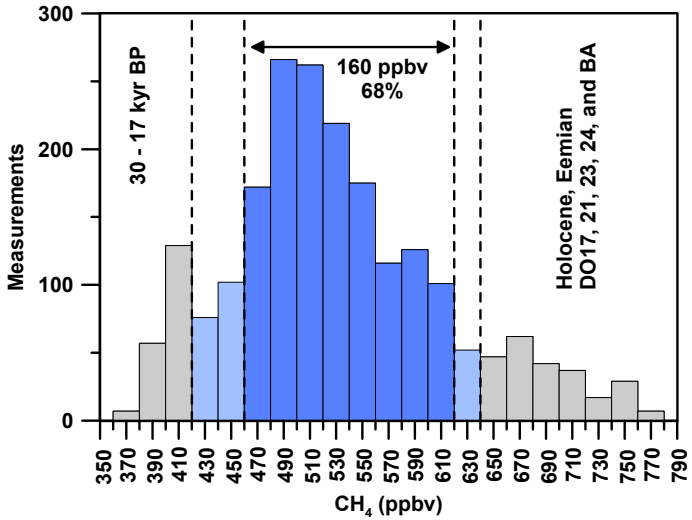

Fig. 2. Histogram of NGRIP methane measurements over the last glacial cycle (120–10 kyr BP). 68 % of all measurements (dark blue) have a concentration between 460 and 620 ppbv with the most frequent concentration to be found around 500 ppbv. Concentrations below 420 ppbv are only found in the time interval between 30–17 kyr BP around the LGM. Excluding the Holocene and the end of the Eemian, concentrations higher than 640 ppbv occur only in DO events 17, 21, 23, 24, and the BA.

CPD
9, 4655–4704, 2013

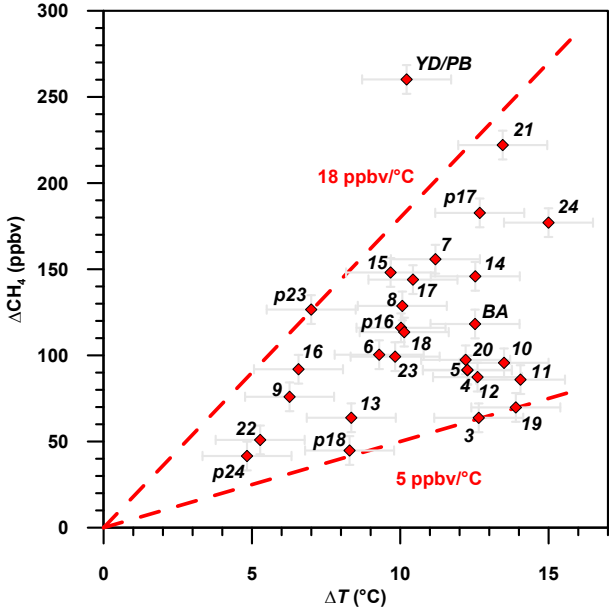

Fig. 3. Comparison of methane and NGRIP temperature amplitudes at the fast DO event increases. The calculations are done as described in Sect. 3.2. Names of DO events and other peaks are displayed in italics. Events with names starting with "p" always precede the main event with the indicated number. The red dashed lines show the enveloping minimum and maximum sensitivities observed for DO events during the last glacial.

CPD
9, 4655–4704, 2013

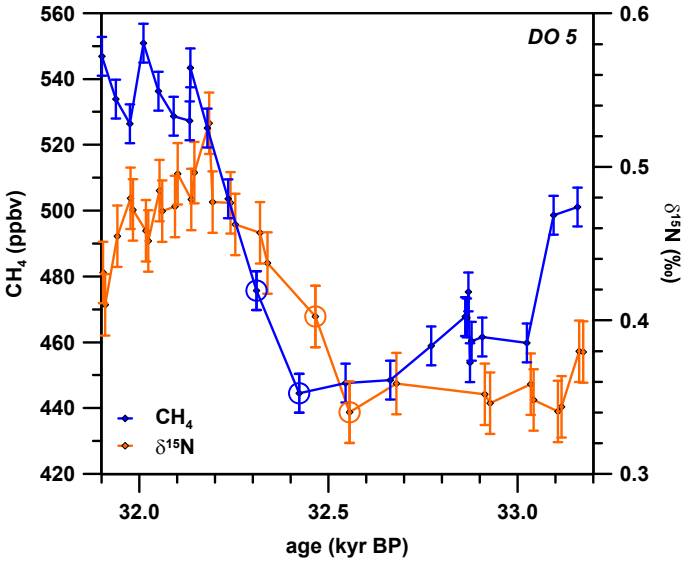

Fig. 4. Timing of CH_4 and $\delta^{15}N$ for DO event 5. CH_4 from NGRIP in blue, $\delta^{15}N$ (Kindler et al., 2013) in orange measured on the same ice core. The selected data points, where the first increase is visible, are indicated by open circles.

CPD
9, 4655–4704, 2013

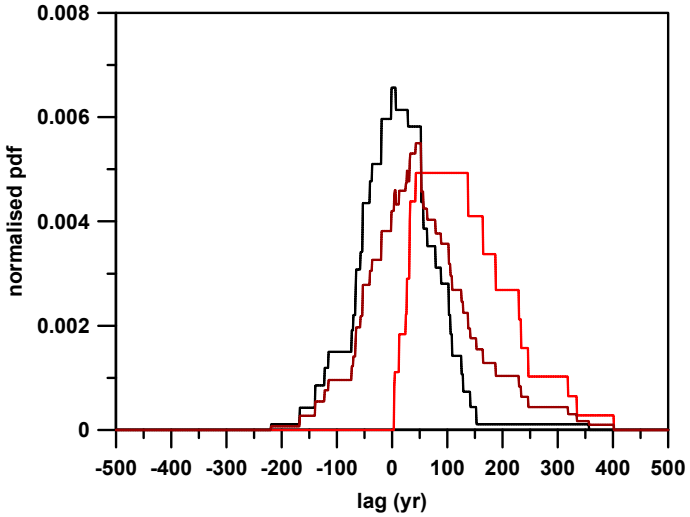

Fig. 5. Normalised probability density function (pdf) of lags between methane and NGRIP temperature for DO events showing a significant lag (red), for DO events showing no significant lag (black), and for all DO events together (brown).

CPD
9, 4655–4704, 2013

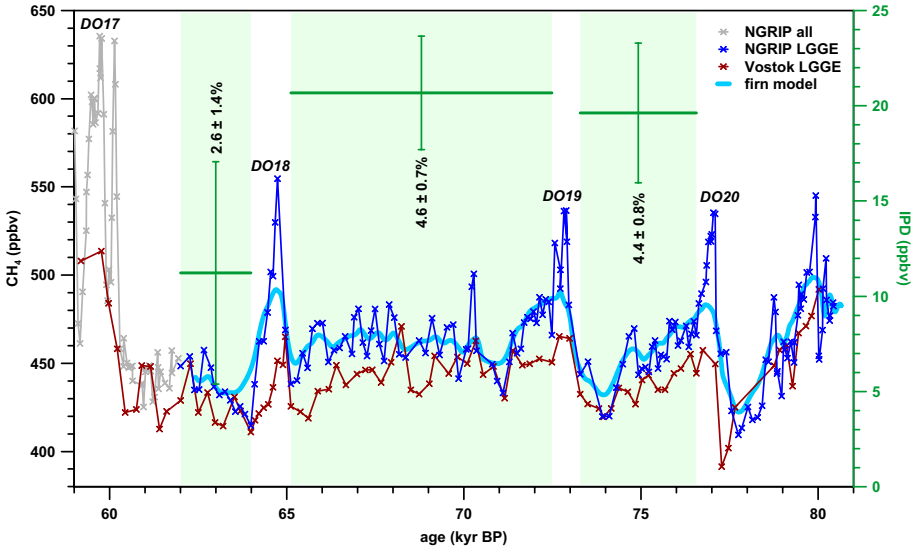

Fig. 6. Interpolar concentration difference of methane calculated in the stadial periods between 80–60 kyr BP. The samples from Greenland (new data from NGRIP in blue) and Vostok (red, Bender et al., 2006) have been measured during the same measurement series and in the same laboratory (LGGE Grenoble). The absolute interpolar concentration difference (IPD) is shown in green, the relative interpolar concentration difference (rIPD) is given in numbers. The methane data from NGRIP which are not from LGGE and shown in grey (new data and Huber et al., 2006) are shifted to the LGGE scale in this plot (see Sect. 2 for details to the offset corrections). The thick blue line represents the firn model output (Schwander et al., 1993; Spahni et al., 2003), where the NGRIP data have been attenuated to Vostok conditions.

CPD
9, 4655–4704, 2013

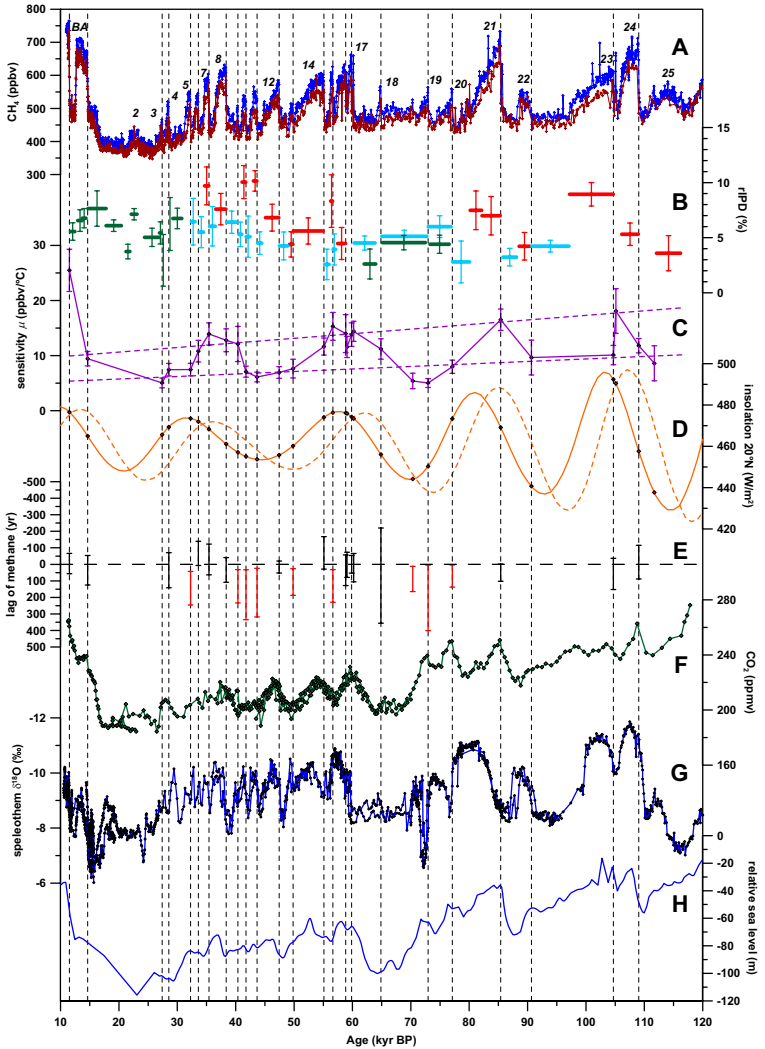

CPD
9, 4655–4704, 2013

NGRIP methane record

M. Baumgartner et al.

Fig. 7. Variations in the methane-to-NGRIP temperature sensitivity μ and timing of the fast DO event increases. **(A)** Atmospheric CH_4 concentration from NGRIP (blue, Baumgartner et al., 2012; Capron et al., 2010b, 2012; Schilt et al., 2010b; Huber et al., 2006; Flückiger et al., 2004, and new data) and merged records from EDML (Baumgartner et al., 2012; Schilt et al., 2010b; Capron et al., 2010b; EPICA Community Members, 2006) and TALDICE (Buiron et al., 2011; Stenni et al., 2011; Schilt et al., 2010b) ice cores in red; **(B)** rIPD from Baumgartner et al. (2012) and new data from this study over the DO events 18–20 in green, rIPD (after application of offset corrections) based on NGRIP and merged EDML and TALDICE in red (interstadial) and blue (stadial); **(C)** CH_4-to-NGRIP temperature sensitivity (μ), the dashed lines are the regressions through high- and low sensitivity states; **(D)** northern summer insolation (JJA, solid line) evaluated at the ages of the DO events (orange diamonds) and spring insolation (AMJ, dashed line) at 20° N (Quinn et al., 1991); **(E)** lag of the fast CH_4 concentration increases and NGRIP temperature increase as it is visible in the comparison of CH_4 and $\delta^{15}N$ (Kindler et al., 2013), the events marked with red show lags significantly different from zero; **(F)** atmospheric CO_2 concentration from EDML and TALDICE (Bereiter et al., 2012; Lüthi et al., 2010), EPICA Dome C (Monnin et al., 2001), and the Byrd ice core (Ahn and Brook, 2007, 2008); **(G)** speleothem $\delta^{18}O$ from Hulu and Sanbao cave (Wang et al., 2001, 2008), Hulu cave values are shifted by +1.6 ‰ to match the Sanbao values (Wang et al., 2008); **(H)** smoothed version of the sea level record (Rohling et al., 2009; Grant et al., 2012). Speleothem and sea level records are shown on their original time scales, the other records are on the gas age scale calculated by Kindler et al. (2013) based on the ss09sea06bm ice age scale (NGRIP Project Members, 2004; Andersen et al., 2006; Johnsen et al., 2001). The CO_2 records have been brought on the same age scale by CH_4 synchronisation – see **(A)**.

CPD
9, 4655–4704, 2013

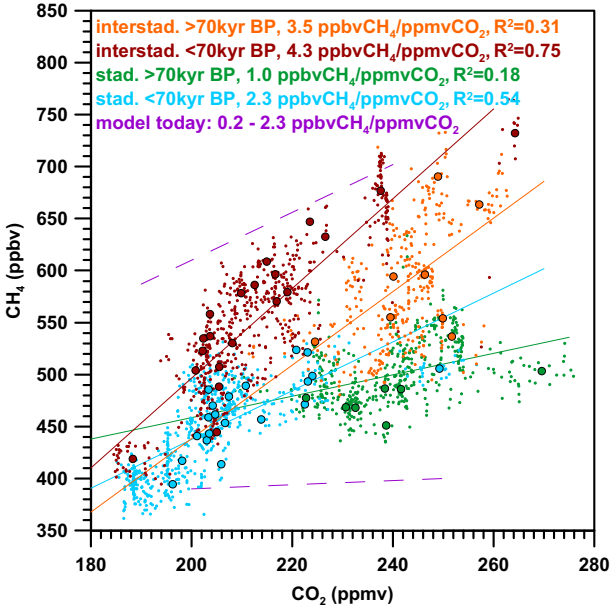

Fig. 8. Comparison of methane and carbon dioxide concentrations during stadial and interstadial periods of the last glacial. NGRIP CH_4 data points plotted against CO_2 concentration (interpolated from merged CO_2 record, Bereiter et al., 2012; Lüthi et al., 2010; Ahn and Brook, 2007, 2008; Monnin et al., 2001). The large points represent the mean stadial/interstadial levels. The estimated range of the effect of a CO_2 increase on wetland CH_4 emissions from models based on today's conditions are indicated by the purple dashed lines (Melton et al., 2013), where the intercept with the ordinate was chosen arbitrarily. The results of the linear regression, which is based on the small data points, are given in the legend of the figure.

CPD
9, 4655–4704, 2013

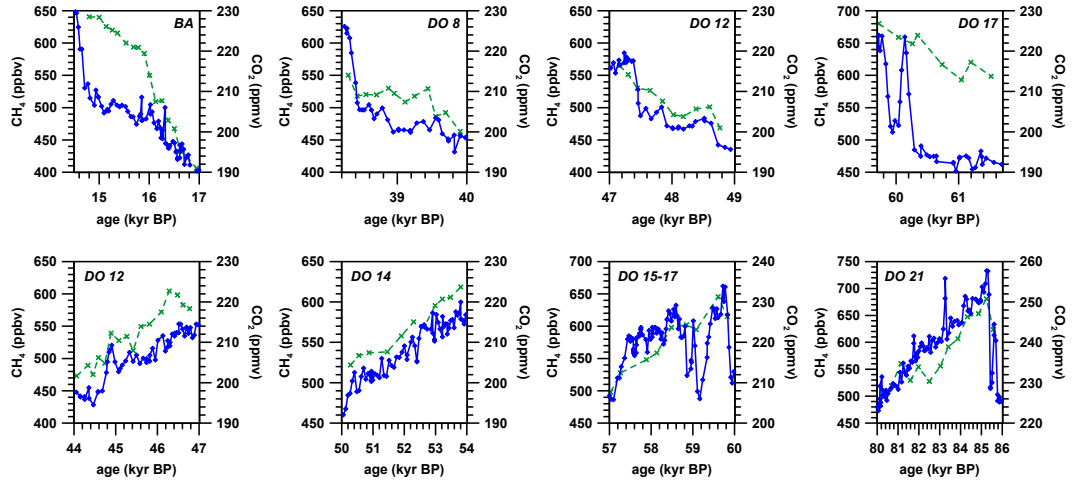

Fig. 9. Covariance of trends in methane and carbon dioxide concentrations in specific time intervals. CH_4 from NGRIP in blue, and CO_2 in green (Bereiter et al., 2012; Lüthi et al., 2010; Ahn and Brook, 2007, 2008; Monnin et al., 2001). The upper panels show the slow increases of CH_4 and CO_2 preceding the BA, and the DO events 8, 12, and, 17. The lower panels show the slow decreases of CH_4 and CO_2 during the DO events 12, 14, 17–15, and 21. Note the different scalings of the x-axes and the offsets in the y-axes.

CPD
9, 4655–4704, 2013